FISEVIER

Contents lists available at ScienceDirect

European Journal of Medicinal Chemistry

journal homepage: www.elsevier.com/locate/ejmech



Research paper

In silico discovery and mechanistic profiling of STING agonists engaging the transmembrane domain

Ahmad Junaid ^{a,1}, Uddav Pandey ^{a,1}, Janine Ward ^{a,1}, Nilesh Meghani ^a, Shannon Miller ^a, Austin Negron ^a, Kendal Ryter ^a, David Burkhart ^a, Nobuyu Mizuno ^b, Victor R. DeFilippis ^b, Omer Rasheed ^{a,*,1}

ARTICLE INFO

Keywords: Stimulator of interferon genes (STING) Transmembrane domain (TMD) Cytosolic cyclic dinucleotide (CDN) STING agonists Immunotherapy Innate immune

ABSTRACT

Stimulator of interferon genes (STING) is an ER resident cytosolic pattern recognition receptor involved in innate immune signaling and is a promising therapeutic target in immuno-oncology and vaccine adjuvant design. While canonical STING agonists typically activate the receptor via direct engagement with the cytosolic cyclic dinucleotide (CDN)-binding domain (CBD), recent high-resolution structural studies have uncovered a distinct allosteric binding site within the transmembrane domain (TMD). Here, we report the identification and characterization of a novel STING agonist, compound 7k, which uniquely engages the TMD rather than the cytosolic domain. Through comparative molecular docking and binding site validation, the TMD of STING was computationally identified as the preferential site of engagement, diverging from the classical CBD. This mode of activation is functionally significant, as it leads to a demonstrably distinct set of downstream molecular phenotypes. Furthermore, our study led to the discovery of structurally related series of potent, small-molecule human STING activators with potential utility as immunomodulatory therapeutics. A lead compound, 7k, emerged with potent STING-dependent activity in vitro and displayed adjuvant efficacy in vivo, as shown by enhanced antigen-specific IgG production and Th1/Th2 cytokine responses in a genetically humanized STING mouse model. These findings support the TMD as a druggable allosteric site and highlight 7k as a promising candidate for next-generation STING-targeted immunotherapeutics.

1. Introduction

Molecular docking

The innate immune system is vital to protecting hosts from proliferative threats such as microbial infection and cancer. This is rapidly initiated following detection of pathogen- and danger-associated molecular patterns (P/DAMPs) by germline encoded pattern-recognition receptors (PRRs) [1–3]. The **stimulator of interferon genes (STING)** protein is a cytosolic PRR that detects cyclic dinucleotides (CDNs) and acts as a critical adaptor in the cyclic GMP–AMP synthase (cGAS) signaling cascade. Upon recognition of cytosolic double-stranded DNA, cGAS catalyzes the formation of 2'3'-cyclic GMP–AMP (cGAMP), a second messenger that directly binds to and activates STING [4–6]. The cGAS–STING axis plays an essential role in the host immune defense and is activated in response to a variety of viral [7] and bacterial [8]

infections as well as transformed cells [9]. STING activation leads to recruitment and phosphorylation of TANK-binding kinase 1 (TBK1), which subsequently phosphorylates transcription factors interferon regulatory factor 3 (IRF3) and nuclear factor κB (NF- κB). These transcription factors translocate to the nucleus, where they induce the expression of type I interferons (IFN–I) and proinflammatory cytokines [10,11]. These cytokines orchestrate the regulation of co-stimulatory molecules and antimicrobial effectors, thus bridging innate and adaptive immune responses. Pharmacologic activation of STING has demonstrated therapeutic promise across multiple preclinical models, including cancer immunotherapy, infectious diseases, and vaccine adjuvanticity [12–17]. STING activation has been shown to enhance antigen presentation, support cytotoxic T cell priming, and promote both humoral and cellular immune responses, key

^a Inimmune Corporation, Missoula, MT, United States of America

b Vaccine and Gene Therapy Institute, Oregon Health and Science University, Beaverton, OR, United States of America

^{*} Corresponding author.

E-mail address: omer.rasheed@inimmune.com (O. Rasheed).

 $^{^{1}\,}$ Investigators contributed equally to this work.

features of an effective vaccine adjuvant [18–20]. As a result, STING agonists are being actively explored as adjuvants that can improve vaccine potency, breadth, and durability, particularly in the context of subunit and inactivated vaccines [21].

Historically, STING therapeutic development has been dominated by CDN analogs and non-CDN small molecules designed to target the CDNbinding domain (CBD). Prominent CDN agonists, such as ADU-S100 [22, 23] and MK-1474 [24], demonstrate effectiveness in preclinical models; however, their application is limited by poor membrane permeability, rapid enzymatic degradation, and suboptimal drug-like properties. To overcome these challenges, attention has turned to non-CDN small molecules, which offer improved pharmacokinetic properties and greater flexibility for medicinal chemistry optimization [25–28]. This is exemplified by DMXAA, a flavone-based murine STING agonist with robust antitumor, antiviral, and adjuvant activity [29]. Although efficacious in mice, they fail to activate human STING due to species-specific structural differences [20,30-32]. More recent efforts have produced cross-reactive non-CDN agonists, such as diABZI (GSK), a dimeric amidobenzimidazole [33] with systemic efficacy in murine tumor models, and MSA-2 (Merck) [27], an orally bioavailable non-nucleotide dimer that stabilizes human STING in a closed-lid conformation. Additional candidates include SR-717 (Scripps) [34], HG381 (HitGen) [35], and SNX281 (Silicon Therapeutics) [36] shown in Fig. 1. While promising, many of these agents still target the canonical cytosolic binding pocket, which remains subject to interspecies variation and structural constraints.

An emerging and increasingly promising strategy for modulating STING activity involves targeting a cryptic binding site located within its transmembrane domain (TMD). In contrast to the well-characterized CBD, which is situated in the cytosolic region of STING, the four pass TMD is embedded in the endoplasmic reticulum membrane and comprises a helical bundle that plays a central role in receptor activation. Recent cryo-electron microscopy (cryo-EM) studies have revealed that small molecules such as C53 engage this membrane-associated interface by binding between adjacent transmembrane helices in a partially solvent-exposed, hydrophobic groove [37–40]. Ligand binding at this site induces conformational changes that stabilize the active form of STING and promote its oligomerization, an essential step for full downstream signaling. In addition to providing an alternative mode of

STING activation, the TMD offers several practical and pharmacological advantages. These include improved membrane permeability, reduced species-specific variability in target engagement and activation (i.e., compounds binding the TMD tend to show more consistent activity across STING orthologs in different species compared to CBD ligands), and greater flexibility for allosteric modulation. Collectively, these features make the TMD an attractive and feasible target for the development of next-generation STING agonists, especially where traditional CBD-directed approaches have faced pharmacokinetic or translational limitations [41–44]. At the same time, prior examples such as C53 highlight key challenges, including species-restricted activity (limited to human STING), partial dependence on cGAMP co-stimulation, and a lack of comprehensive in vivo pharmacology. These limitations underscore the need to identify new chemotypes that can better exploit the TMD while overcoming these drawbacks.

2. Results and discussions

Previous work identified a novel small molecule activator of human, but not mouse, STING called G10 (Fig. 1) [45,46]. The potency of this molecule was low and, as such, we adopted a cheminformatic approach to improve the potency, pan-isoform selectivity and physiochemical properties of the G10 pharmacophore against human STING with better understanding of the binding region of these molecules. To explore the structural determinants of STING agonism and guide the rational design of new analogs, a structure-based computational approach was undertaken.

2.1. Computational docking and binding site assessment

To explore the potential binding modes of **G10** and its STING analogs, comparative molecular docking studies were carried out targeting the CBD or TMD regions of the STING protein. Docking to the CBD was performed using the X-ray crystal structure of human STING in complex with the synthetic agonist diABZI (PDB ID: 8STH), while TMD docking utilized the cryo-EM structure of STING co-crystallized with the non-canonical agonist C53 (PDB ID: 7SII). To validate the reliability of the docking protocol, each co-crystallized ligand was redocked into its respective site. The resulting root-mean-square deviation (RMSD) values

Fig. 1. Known examples of cyclic dinucleotide (CDN)-based ligands non-CDN based ligands.

were below 0.5 Å, indicating excellent agreement with the experimentally observed binding poses and validating the robustness of the docking methodology.

Initially, **G10** was docked into both the canonical CBD and the TMD of STING (Fig. 2A and C). At the TMD site, **G10** adopted a conformation closely resembling the C-shaped binding pose of the non-canonical agonist C53 and maintained key interactions, notably a hydrogen bond with Tyr106 (Fig. 2B). In contrast, molecular docking at the CBD revealed that although **G10** maintained hydrophobic interactions with Tyr167 [47], it failed to reproduce key hydrogen bonding interactions with Ser162 and Thr263, which are also essential for STING activation (Fig. 2D). These finding indicate that **G10** preferentially binds to TMD, suggesting this site as primary site for its STING agonist activity.

2.2. First-generation analogs: synthesis and functional evaluation

To elucidate structural determinants underlying STING agonism, we examined two 1-oxo derivatives of **G10**, **7a** and **7b**, that invert the donor–acceptor geometry of the central pharmacophore, thereby misaligning both the carbonyl and NH groups. Literature reports have demonstrated that substituting the thio moiety with its bio-isosteric analog, a carbon, can lead to improved biological activity [48]. Therefore, we decided to include that version in our studies as well.

The synthesis of the target benzothiazine derivatives was carried out through a modular three-step sequence, as depicted in Scheme 1. Unless otherwise stated, all starting materials are commercially available. For some analogs, the 1,4-benzothiazine core (3) was synthesized in-house via cyclization of methyl anthranilate with carbon disulfide under basic conditions. In other cases, the compounds were prepared by treating methyl 2-oxo-2H-1,4-benzothiazine carboxylate or 1-oxo-2H-1,4-benzothiazine carboxylate (3) with substituted benzyl bromide gave compound (4), which underwent a hydrolysis reaction to give the key intermediate. Final compounds were obtained by coupling these acids with a diverse set of aryl methylamines under standard amide bond-forming conditions to give the corresponding compound (6)

respectively in good to excellent yields. All intermediates and final products were purified by silica gel chromatography, and their structures were confirmed by NMR and mass spectrometry. Several analogs were synthesized using a generalized synthetic route (Scheme 1).

Docking analysis of 7a and 7b (Fig. 3A) were performed at both the CBD and TMD sites. Within the CBD, both analogs exhibited similar binding poses and hydrophobic contact patterns to those of G10, suggesting that if this site were the principal determinant of activity, these compounds might be expected to retain biological function. However, in vitro assays revealed a complete loss of STING activation, implying that CBD binding is insufficient to drive functional response in this chemotype. Strikingly, docking of 7a and 7b at the TMD site revealed a markedly altered binding mode. Unlike G10 and C53, these analogs failed to adopt the characteristic C-shaped conformation. Instead, they assumed a flipped orientation that disrupted optimal packing within the pocket and abolished the key hydrogen bond interaction between the core carbonyl and Tyr106. This interaction was previously identified as critical for productive TMD engagement (Fig. 3B and C). These findings are consistent with the observed lack of in vitro activity (Fig. 3D) and underscore the importance of correct spatial orientation and interaction geometry within the TMD as a determinant of functional STING activation.

2.3. Second-generation analogs: positional substitutions and SAR insights

To assess the tolerance of the TMD bind site to substituent positioning, analogs incorporating shifts of the furan ring were synthesized following the general procedure in Scheme 1. Specifically, 7c, 7d, and 7e each featuring a positional shift of the furan ring from the original 7-position, were prepared (Fig. 4A). These analogs were found to be inactive in the cellular assay (Fig. 4B).

Computational docking analysis revealed that this structural modification disrupted the ligands' ability to adopt the characteristic C-shaped conformation associated with productive binding at the TMD site. While some peripheral interactions with residues such as Leu123,

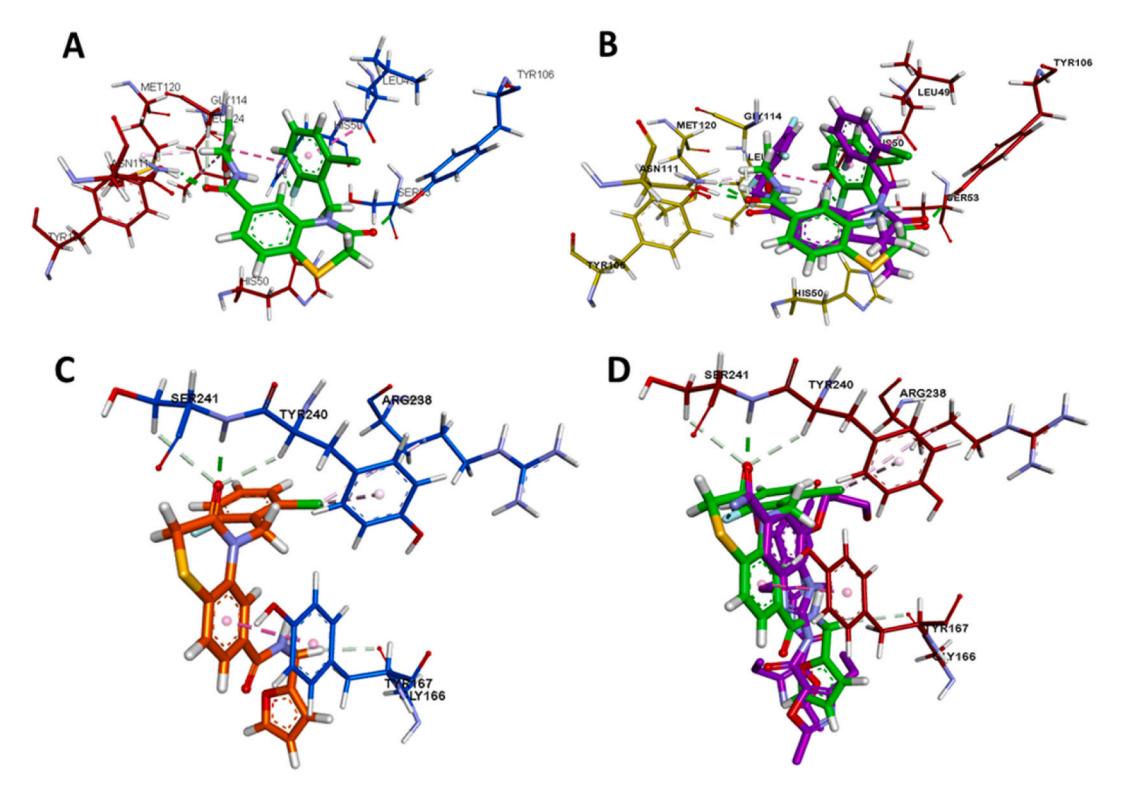


Fig. 2. Molecular docking poses of G10 within the STING protein domains; A) Binding pose of G10 within the TMD; B) Superimposition of G10 and the reference TMD-binding compound C53, (C) Docking pose of G10 within the CBD; D) Overlay of G10 with the canonical STING agonist diABZI in the CBD.

Scheme 1. General scheme for the synthesis of compounds.

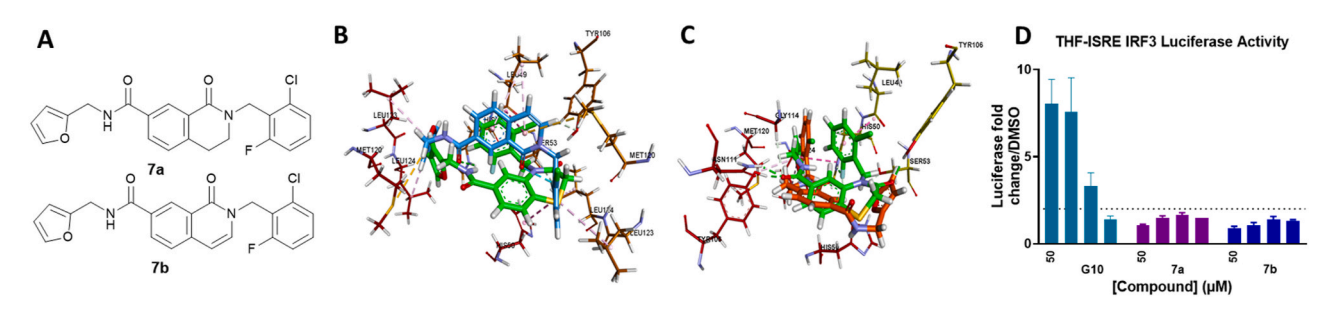


Fig. 3. Comparison of TMD docking poses and cellular activity of compounds G10, 7a and 7b; A) Compounds 7a and 7b; B) Overlay of docking poses for 7a and G10 within the STING TMD; C) Superimposition of 7b and G10 within the TMD; D) Luciferase activity results of 7a and 7b in human THF cells. The assay measured relative luminescence units (RLU) for each compound at 50 μ M, 35 μ M, 12.5 μ M and 6.25 μ M. Triplicate values were averaged and normalized to luciferase activity of 1 % DMSO. Luciferase fold-change relative to DMSO was plotted using Prism. Compounds were considered active if they induce \geq 2-fold luciferase activity compared to DMSO. G10 was included as a positive control.

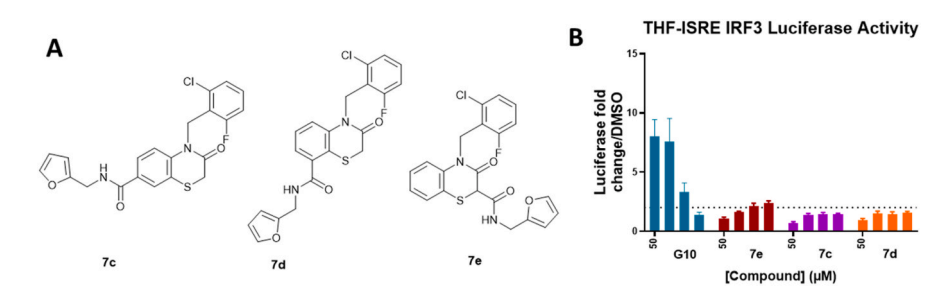


Fig. 4. A) Compounds 7c, 7d and 7e; B) THF luciferase reporter assay by 7c, 7d, 7e and G10. The assay measured average relative luminescence units (RLU) for each compound at 50 μ M, 35 μ M, 12.5 μ M and 6.25 μ M. The values were averaged across triplicates and normalized to the luciferase activity of 1 % DMSO. Fold-change in luciferase activity relative to DMSO was plotted using Prism. Compounds were considered active if they induce \geq 2-fold luciferase activity compared to DMSO. G10 was included as a positive control.

Met120, and Ser53 were retained, the central pharmacophoric alignment was lost, and the critical hydrogen bonding network was not maintained (Fig. S1). These observations provide a structural rationale for the lack of *in vitro* STING activation and highlights the importance of precise spatial positioning of key substituents to preserve conformational fidelity required for TMD engagement. Collectively, these findings suggest that the TMD of the STING receptor is the most probable binding site for **G10**-based analogs.

2.4. Targeted substitutions and discovery of 7k

Guided by this mechanistic insight, we next pursued structural optimization through a focused structure–activity relationship (SAR) investigation. This effort systematically evaluated the impact of strategic substituent modifications on biological activity, with the objective of delineating molecular features critical for potency, selectivity, and receptor engagement. Fig. 5A summarizes the compounds synthesized based on our computational studies targeting the TMD region, with the aim of enhancing agonistic efficacy and optimizing the pharmacophoric

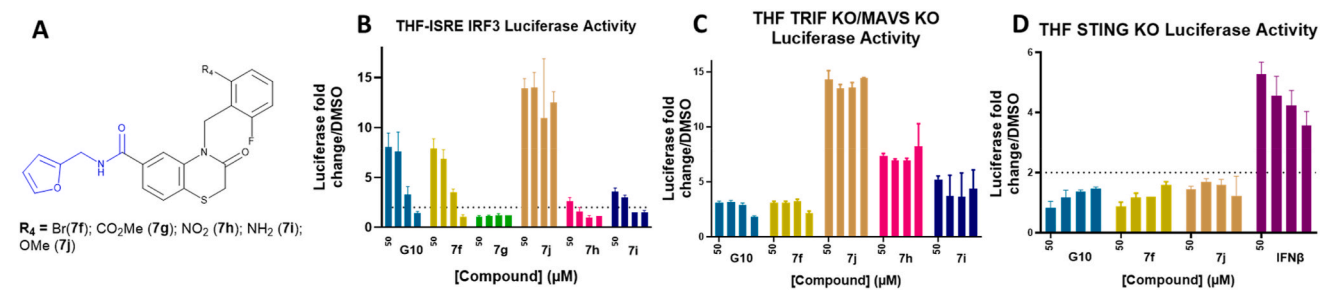


Fig. 5. A) Compounds 7f, 7g, 7h, 7i and 7j; B) Luciferase activity results of 7f, 7g, 7j, 7h, 7i and 7j in human THF cells. The assay measured average relative luminescence units (RLU) for each compound at 50 μM, 35 μM, 12.5 μM and 6.25 μM. The values were averaged across triplicates and normalized to the luciferase activity of 1 % DMSO. Fold-change in luciferase activity relative to DMSO was plotted using Prism. Compounds were considered active if they induce \geq 2-fold luciferase activity compared to DMSO. 7g was excluded from further evaluation. C) STING specificity in human THF-ISRE TRIF/MAVS $^{-/-}$ cells, assessed using the same procedure as B. Compounds 7h, 7i and 7j showed significant luciferase activity through the human STING pathway. G10 was the positive control for both assays in B and C. D) Luciferase activity in THF-ISRE STING $^{-/-}$ cell to confirm STING specificity. None of the tested candidates shown luciferase activity using the TRIF/MAVS pathway. IFNβ was used as a positive control.

profile of the series. Among these synthesized analogs in the first series, 7f, incorporating a 6-fluoro group and a 2-bromo substitution, retained STING activity, suggesting that the receptor tolerates bulkier halogens at the 2-position. In contrast, 7g, bearing a methyl ester at the 6-position, exhibited no agonistic activity, implicating poor accommodation of polar ester groups at this site and underscoring a preference for halogenbased substituents, likely due to favorable van der Waals or halogen bonding interactions (Fig. 5B). To further probe the electronic tolerance of the 6-position, we evaluated polar substituents including nitro (7h), amine (7i), and methoxy (7i). Both nitro and amine analogs showed minimal activity, while 7i demonstrated markedly enhanced potency (Fig. 6B). Furthermore, evaluation in TRIF/MAVS KO (TRIF/MAVS^{-/-}) and STING KO (STING^{-/-}) cell lines confirmed that the observed activity of these compounds is STING-dependent (Fig. 5C and D). These findings suggest that optimal STING activation depends on a delicate balance of hydrogen bonding potential, polarity, and steric fit, with the methoxy group offering an advantageous profile.

To enhance hydrophobic interactions and leverage the inductive effects of fluorine atoms, the furyl group of the G10 scaffold was replaced with a trifluorobenzyl substituent [48]. A series of analogs, 7m (amine), 7n (nitro), 7l (methoxy) were synthesized following the general synthetic scheme (Scheme 1; Fig. 6A). Compound 7k were synthesized by treating compound 7l with BBr₃ in DCM. These compounds were screened for luciferase activity and subsequently screened for human STING agonistic activity (Fig. 6B). Among these, 7k exhibited the most potent activity, likely due to a stabilizing hydrogen bond interaction facilitated by the hydroxyl group, which may enhance ligand–receptor binding within the transmembrane domain (Fig. 6).

To elucidate the structural basis for these observations, molecular

docking studies were performed at both the TMD and CBD. At the TMD site, 7k exhibited a stabilizing hydrogen bond with Ser53, absent in the parent G10, correlating with enhanced bioactivity (Fig. 7). 7l (methoxy), 7n (nitro), and 7m (amine) also showed favorable noncovalent interactions, including alkyl- π contacts and electrostatic complementarity, supporting their activity profiles (Fig. S2). In contrast, docking to the CBD revealed no significant additional interactions, reinforcing the notion that G10-based analogs predominantly exert their effects via TMD engagement. Docking analysis also revealed the presence of a hydrophobic cavity adjacent to the thiazine core in the TMD region (Fig. 7C), suggesting an opportunity to further enhance binding affinity by introducing methyl substitution at the 6-position of the benzo [b] [1,4]thiazine ring.

To exploit this feature, we introduced a methyl substituent at the 3-position of the benzo[b] [1,4]thiazine ring, hypothesizing that this modification would improve hydrophobic packing and overall receptor engagement. Based on prior SAR data, we selected representative analogs for this targeted optimization. Specifically, 7q (nitro) and 7r (amine), 7p (methoxy) and 7o (hydroxyl) were synthesized using generalized synthesis scheme (Fig. 8). All four compounds demonstrated robust STING agonistic activity, as confirmed in cellular assays (Fig. 8B, C and 8D). Notably, the methylated analogs exhibited superior activity relative to the parent G10 scaffold, providing strong support for the role of the adjacent hydrophobic cavity in mediating productive ligand—receptor interactions. These findings further validate the utility of structure-guided design in fine-tuning agonist potency via TMD engagement.

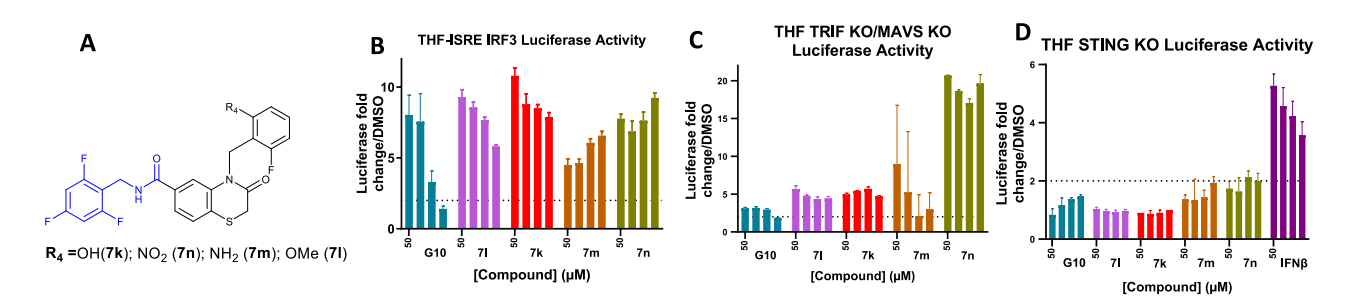


Fig. 6. A) Compounds 7k, 7l, 7m and 7n; B) Luciferase activity results of 7k, 7l, 7m and 7n in human THF cells. The assay measured average relative luminescence units (RLU) for each compound at 50 μM, 35 μM, 12.5 μM and 6.25 μM. The values were averaged across triplicates and normalized to the luciferase activity of 1 % DMSO. Fold-change in luciferase activity relative to DMSO was plotted using Prism. Compounds were considered active if they induce \geq 2-fold luciferase activity compared to DMSO. C) STING specificity in human THF-ISRE TRIF/MAVS $^{-/-}$ cells, assessed using the same procedure as in B. Compounds 7k, 7l, 7m and 7n showed significant luciferase activity through the human STING pathway. G10 was the positive control for both assays in B and C. D) Luciferase activity in THF-ISRE STING $^{-/-}$ cells to confirm STING specificity. None of the candidates shown luciferase activity using the TRIF/MAVS pathway. IFNβ was used as a positive control.

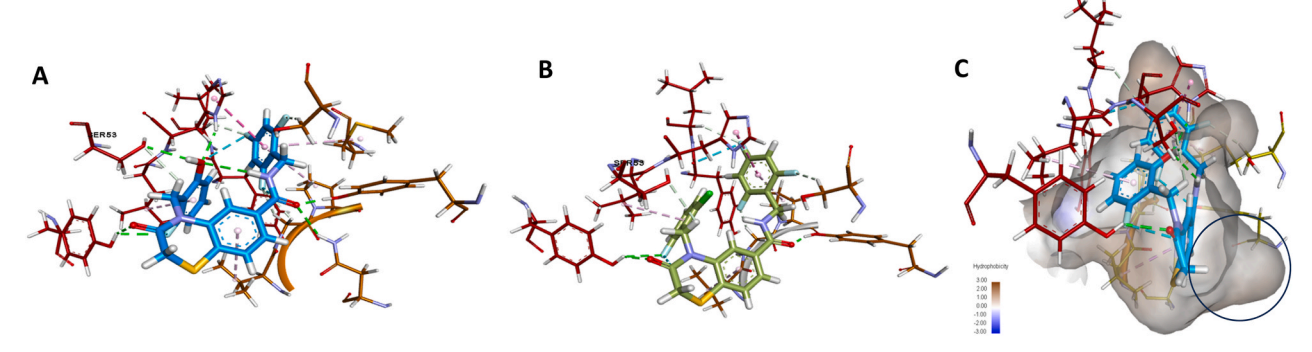


Fig. 7. Docking pose in the TMD of STING receptor, A) 7k (in blue), B) Analog of 7k with hydroxyl replaced with Chlorine (which lacks the SER53 hydrogen bond interaction). C) Hydrophobic receptor surface of STING receptor TMD region with docked 7k.

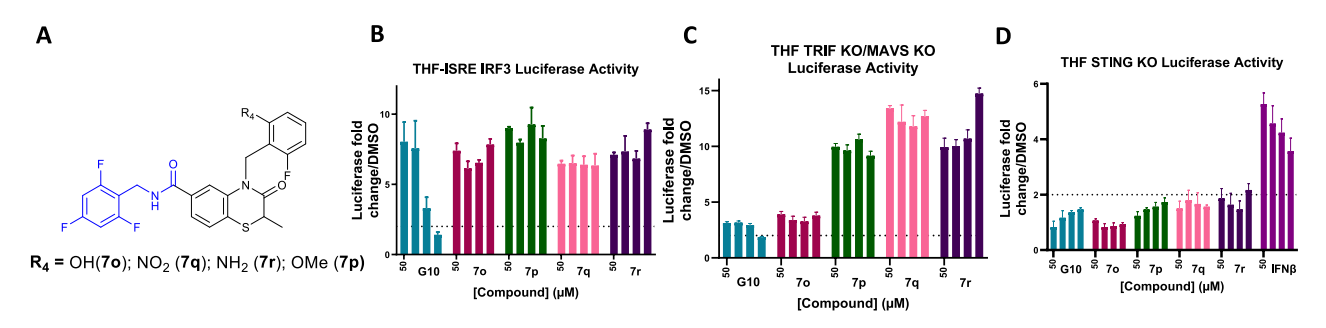


Fig. 8. A) Compounds 7o, 7p, 7q and 7r; B) Luciferase activity results of 7o, 7p, 7q and 7r in human THF cells. The assay measured average relative luminescence units (RLU) for each compound at 50 μM, 35 μM, 12.5 μM and 6.25 μM. The values were averaged across triplicates and normalized to the luciferase activity of 1 % DMSO. Fold-change in luciferase activity relative to DMSO was plotted using Prism. Compounds were considered active if they induce \geq 2-fold luciferase activity compared to DMSO. C) STING specificity in human THF-ISRE TRIF/MAVS^{-/-}cells, assessed using the same procedure as in B. All compounds showed significant luciferase activity through the human STING pathway. G10 was the positive control for both assays in B and C. D) Luciferase activity in THF-ISRE STING^{-/-} cells to determine STING specificity. None of the candidates shown luciferase activity using the TRIF/MAVS pathway. IFNβ was used as a positive control.

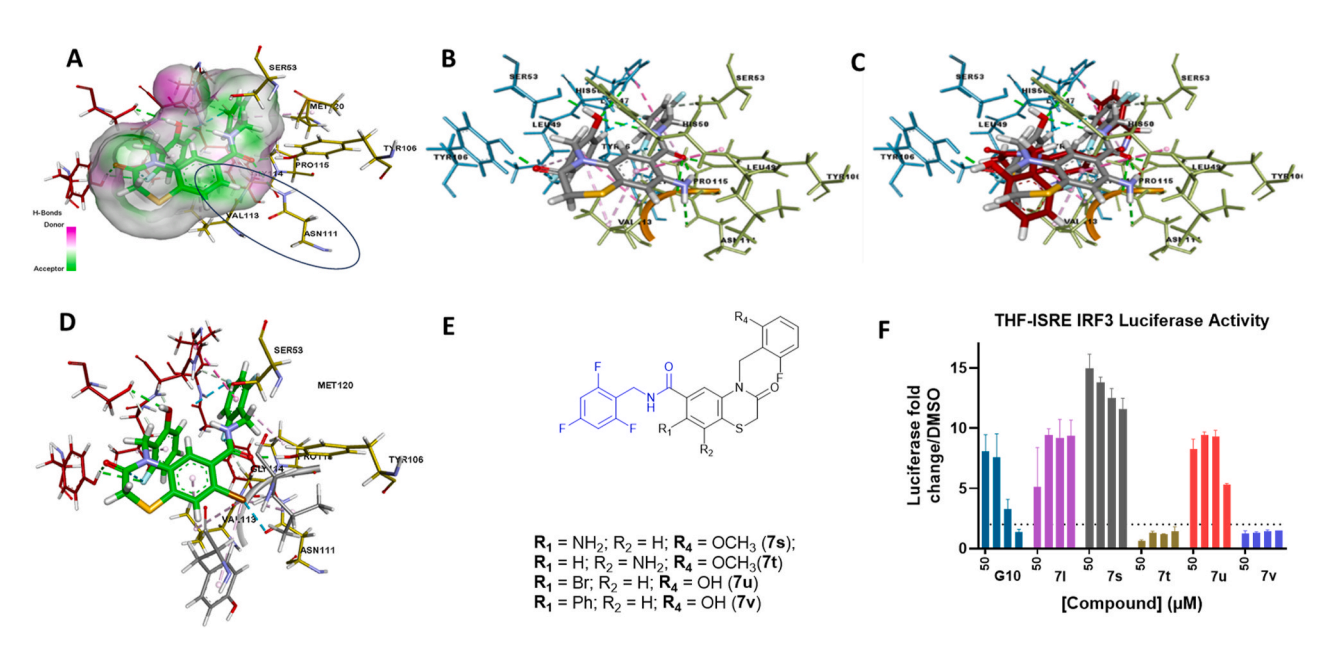


Fig. 9. A) H-bond receptor surface of TMD with 7k. B) Docking pose of 6-amino substituted 7k. C) Docking pose of 5-amino substituted (red) vs 6-amino substituted (grey) 7k. D) Docking pose of bromo-substituted analog 7u; E) Compounds 7s, 7t, 7u and 7v; F) Luciferase activity results of 7l, 7s, 7t, 7u and 7v in human THF cells. The assay measured average relative luminescence units (RLU) for each compound at 50 μ M, 35 μ M, 12.5 μ M and 6.25 μ M. The values were averaged across triplicates and normalized to the luciferase activity of 1 % DMSO. Fold-change in luciferase activity relative to DMSO was plotted using Prism. Compounds were considered active if they induce \geq 2-fold luciferase activity compared to DMSO. G10 was included as a positive control.

2.5. Rational design to probe binding site

To further test our hypothesis that specific interactions within the TMD drive the activity of G10-based STING agonists, we performed targeted binding site analysis using aromatic and hydrogen bond surface maps (Fig. 9). Our aim was to identify nearby residues that could form favorable enthalpic contacts if appropriately positioned functional groups were introduced. The analysis highlighted Asn111 as a potential interaction partner, suggesting that adding a hydrogen bond donor at the 6-position of the benzothiazine core could strengthen binding (Fig. 9A). Supporting this, docking studies revealed that introducing an amino group at the 6-position resulted in a stable hydrogen bond with Asn111 (2.27 Å) while preserving the characteristic C-shaped binding pose (Fig. 9B). In contrast, shifting the amino group to the 5-position led to a flipped binding orientation that disrupted key interactions within the TMD pocket (Fig. 9C). Based on these findings, we hypothesized that the 6-amino-substituted analog would retain STING agonistic activity, whereas the 5-amino variant would exhibit a loss of function.

To experimentally validate this model, we synthesized two analogs 7s and 7t with amino position at 6 and 5 position, respectively (Fig. 9E). 7s retained comparable activity to the active molecule, consistent with our hypothesis. In contrast, 7t, with the amine at the 5-position, lost all activity, reinforcing the importance of spatial placement for TMD engagement (Fig. 9F). Additionally, we also explored whether bulkier groups could be tolerated at the 6-position. A bromo-substituted analog (7u) retained the productive C-shaped conformation and showed additional π -alkyl interactions with Tyr46 (Fig. 9D), suggesting increased steric bulk is compatible with activity. However, when we introduced a phenyl group at the same site (7v), docking showed a disrupted binding pose, and as predicted, the compound was inactive in vitro. Together, these results strongly support our initial hypothesis: that G10-derived compounds exert their agonistic effects through the TMD, and that strategic modifications at the 6-position can meaningfully influence both binding and functional output.

From these collective SAR insights observed across compounds 7a–7v support a ligand-based pharmacophore model for TMD-directed STING agonism. Key features include a central carbonyl group on the benzothiazine core that serves as a hydrogen-bond acceptor, an aromatic/hydrophobic benzyl substituent with an ortho hydroxyl or methoxy group that enhances potency through additional polar interactions, and a small hydrophobic substituent at the 4-position of the core that boosts activity. The 6-position pocket accommodates only small groups such as NH₂ or Br, whereas bulky substituents such as phenyl are not tolerated, consistent with an excluded volume in this region. Together, these features define the minimal pharmacophore required for activity and provide a framework to guide future optimization. For clarity, detailed SAR data for all synthesized analogs (7a-7v), including chemical structures, physiochemical properties, and quantitative parameters, are consolidated in Table S2.

To confirm TMD-specific engagement of 7k, we also conducted a

thermal shift assay (TSA) using the isolated STING cytosolic domain. As detailed in a separate study [49], this cell-free assay did not show any thermal stabilization of the cytosolic domain in the presence of 7k, in contrast to the positive control cGAMP, which robustly increased thermal stability. Additionally, forward genetic studies identified amino acids in the STING TMD that were necessary for 7k-mediated activation of STING signaling, further confirming engagement of this region. These findings are consistent with our docking results and cellular data, reinforcing the conclusion that G10-based analogs do not engage the canonical CBD, but instead act through the TMD to activate STING signaling.

Following the initial 4-point screen shown in Figs. 6 and 8, we expanded testing to an 8-point dilution series to determine EC₅₀ values for the most active compounds. Compounds **70**, **7p**, **7q**, and **7r** displayed EC50 of 1.02 \pm 0.27 $\mu M,~3.28 \pm 0.55~\mu M,~1.45 \pm 0.19~\mu M,$ and 0.85 \pm 0.21 µM, respectively (Fig. 10A). Among the second-generation analogs, 71, 7k, 7m, and 7n exhibited EC50 values of 5.41 \pm 0.60 $\mu M,$ 4.02 \pm 0.94 μ M, 2.28 \pm 0.25 μ M, and 2.41 \pm 0.28 μ M, respectively, while the reference compound G10 was used as positive control (Fig. 10B). Counter-screens in THF-ISRE TRIF/MAVS^{-/-} cells and THF-ISRE STING^{-/-} cells confirmed STING-dependent activity: 7k and 7n showed strong, dose-dependent activation that was lost in STING^{-/-} cells; 7m displayed weaker but still STING-dependent activity, whereas 71 showed minimal activity (Fig. S3). These results demonstrate that the most active analogs engage the human STING pathway selectively, with 7k emerging as the lead candidate for further in vitro and in vivo characterization.

Additionally, to complement our experimental findings, we computationally predicted key ADMET properties of the active analogs using ADMETlab 2.0 [47b]. All compounds displayed physicochemical parameters consistent with drug-like space (MW < 500 Da, logP within the Lipinski range, TPSA <140 Ų), favorable absorption (high predicted intestinal uptake and acceptable oral bioavailability probabilities), moderate distribution (VDss within the expected range), and half-lives consistent with sustained exposure. Importantly, none of the compounds showed a strong liability for CYP3A4 inhibition, the most clinically relevant isoform for drug–drug interactions. Full predicted ADMET values are provided in Table S1 and Fig. S4.

The dose-response profiling of active analogs further corroborated their engagement with STING, with several compounds showing low micromolar EC_{50} values in human THF cells. These potency data along with TSA results demonstrate that these compounds do not stabilize the canonical CBD but instead support engagement of the TMD, in line with SAR and docking analysis. Collectively, these findings highlight an important mechanistic distinction with downstream consequences. Upon canonical LBD activation, STING forms a channel in the Golgi membrane that allows organellar deacidification through luminal proton leakage. This conserved primordial process occurs independently of TBK1 and triggers additional molecular phenotypes with important implications for immune function. First, detection of elevated organellar

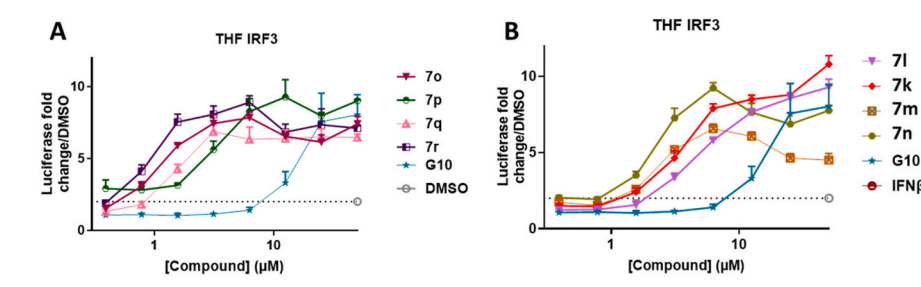


Fig. 10. Dose–response curves of active STING agonist analogs in human THF cells. Compounds were tested across an expanded concentration range, and luciferase activity was normalized to 1 % DMSO. EC₅₀ values were determined by non-linear regression and are shown as mean \pm SEM of three biological replicates. G10 was used as positive control. A) First-generation analogs 70 (1.02 \pm 0.27 μ M), 7p (3.28 \pm 0.55 μ M), 7q (1.45 \pm 0.19 μ M), and 7r (0.85 \pm 0.21 μ M). B) Second-generation analogs 7l (5.41 \pm 0.60 μ M), 7k (4.02 \pm 0.94 μ M), 7 m (2.28 \pm 0.25 μ M), and 7n (2.41 \pm 0.28 μ M), compared with the reference agonist G10 (15.78 \pm 3.47 μ M).

pH by vacuolar ATPase (V-ATPase) leads to induction of noncanonical LC3B-mediated autophagy. Next, cytosolic protons lead to secretion of IL-1 β and pyroptosis through activation of the NLRP3 inflammasome. Finally, proton leakage stimulates lysosomal biogenesis through deactivation of the kinase mTORC1 which induces TFEB, a transcription factor responsible for expression of genes involved in this process. Activation of STING following agonist engagement of the TMD impairs proton efflux, even in the presence of LBD agonism. As such, while TMD agonists elicit typical TBK1-dependent IFN-I responses, they fail to induce TBK1-independent responses such as autophagy, lysosomal biogenesis, and inflammasome activation [49].

2.6. In vivo evaluation of vaccine adjuvanticity

Given its robust *in vitro* performance, favorable synthetic accessibility, and human STING selectivity, 7k was selected as the lead candidate for in vivo immunogenicity studies in a vaccine setting. 7k is a human-selective STING agonist. Therefore, to characterize the immune response to 7k, we utilized C57BL/6 humanized STING (huSTING) mice, in which the murine STING coding region has been replaced with that of the wildtype human allele. huSTING mice (n=8 per group) were left unimmunized or intramuscularly immunized and boosted at a two-week interval with either detergent-split A/Victoria/210/2009 (H3N2, A/Vic) alone or in combination with 7k formulated in DMSO. Two weeks postboost, serum and spleens were collected to evaluate A/Vic-specific IgG titers and Th cell responses, respectively. Inclusion of 7k resulted in significantly higher levels of A/Vic-specific IgG1, IgG2, and total IgG in the serum as compared to mice immunized with A/Vic alone (Fig. 11A).

In line with this, stimulation of splenocytes from these mice with A/Vic resulted in significant increases in the production of Th1- (IFN- γ) and Th2- (IL-4, IL-5) associated cytokines (Fig. 11B). Taken together, these results demonstrate that the inclusion of the STING agonist **7k** significantly enhances antigen-specific Th1- and Th2-biased antibody and T cell responses.

3. Conclusion

In this study, we employed a structure-guided approach to optimize the human-selective STING agonist G10, leading to the development of more potent analogs with improved pharmacological properties. Through comparative molecular docking combined with focused SAR, we identified that this chemotype preferentially interact with TMD of STING, in contrast to the canonical CBD. Thermal shift assays and in silico binding profiles further validated that the agonistic effect of these compounds occur through TMD engagement, not CBD binding. Structure-activity relationship studies revealed that subtle modifications at the 6-position of the benzothiazine core significantly influenced binding affinity and functional activity via TMD interactions. Cellular assays using THF-ISRE reporter lines, along with TRIF/MAVS and STING knockout models, confirmed STING-dependent activity for several analogs, with 7k emerging as the top candidate based on potency, specificity, and synthetic tractability. 7k significantly enhanced both Th1and Th2-associated cytokine responses, as well as antigen-specific IgG production, in a huSTING mouse model when used as a vaccine adjuvant. Collectively, these results establish the TMD as a viable and druggable site for STING activation and highlight 7k as a promising lead

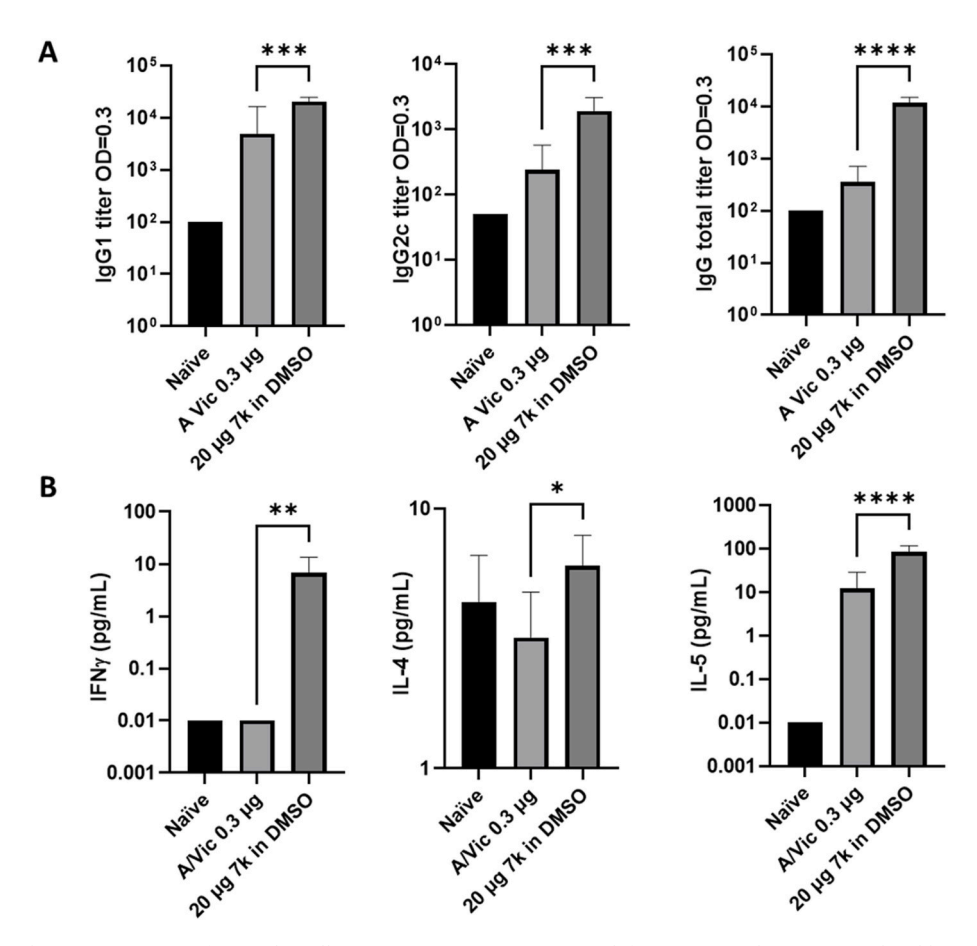


Fig. 11. Inclusion of 7k enhances antigen-specific B and T cell responses. Mice (8/group) were left unimmunized or immunized and boosted 14 days apart with A/Vic alone or in combination with 20 μ g 7k in DMSO. A) Serum was harvested two weeks post-boost and A/Vic-specific antibodies were measured by ELISA. B) Splenocytes were also harvested and restimulated with A/Vic for 72 h. Supernatants were harvested and T cell associated cytokines were measured by Mesoscale Discovery analysis. Ordinary one-way ANOVA statistical analysis; * = p \le 0.05,** = p \le 0.01,*** = p \le 0.001,*** = p \le 0.0001.

for the development of next-generation immunotherapeutics and vaccine adjuvants. Future development of **7k** will require comprehensive PK/PD and safety profiling, mitigation of cytokine release risks, and optimization of formulation and delivery strategies, which represent important milestones toward clinical translation.

4. Materials and methods

4.1. Chemistry

All reagents and solvents were used without further purification. Reaction progress was monitored using thin-layer chromatography (TLC) on Merck Silica gel 60 F254 plates, with visualization under UV light at 254 nm, followed by staining with either vanillin solution (0.2 g vanillin in 5 mL water, 5 mL ethanol, and 1 mL sulfuric acid) or phosphomolybdic acid (PMA) in ethanol, then heated to develop the spots. Product purity was confirmed to be greater than 95 % based on NMR and HRMS. Proton (1H) and carbon (13C) NMR spectra were acquired on Agilent or Bruker 400 MHz spectrometers, calibrated using TMS or residual solvent peaks as internal standards. High-resolution mass spectrometry (HRMS) was performed on an Agilent 6520 Q-TOF instrument equipped with an electrospray ionization (ESI) source operating in both positive and negative ion modes. Flash chromatography was carried out using Isco or Biotage automated medium-pressure systems with prepacked Buchi silica gel cartridges. Compound 2,3,4 and 5 were prepared following the methods in literature [46].

Amide Coupling: To a stirred solution of a carboxylic acid 5 (1 eq.) in a suitable solvent, such as DCM or DMF (10 mL) was added amine (1.3 eq.) and a coupling reagent *i-e* HATU (2.0 eq.) followed by addition of TEA (2.0 eq.) dropwise to the solution and the mixture allowed to stir at room temperature for 2–3 h. When TLC showed completion of the reaction, the reaction mixture was diluted with ice-cooled water and extracted with EtOAc. The combined organic layers were washed with water and then dried over anhydrous MgSO₄. The solvent was evaporated under reduced pressure to obtain the crude material which was purified by column chromatography using mixtures of EtOAc in heptane as eluent to afford a compound (70–80 % yield). Some of the compounds on addition of the crude product into ice-cooled water were precipitated out and collected using filtration technique. The collected precipitate was washed it with water 3 times and dried in high vacuum for 12 h to use it for next step without further purification.

Methyl ether deprotection: The corresponding compound 71 or 7p (1 eq.) was dissolved in dry dichloromethane using a heat-dried three neck round bottom flask equipped with a magnetic stirrer. This solution was cooled down using ice and acetone, to about $-20\,^{\circ}\mathrm{C}$; then a solution of boron tribromide (1 M in CH₂Cl₂; 3 eq.) was added dropwise. After adding the deprotecting agent, the ice bath was withdrawn to allow the reaction mixture to warm up to room temperature and it was stirred for 1–4 h. The reaction was quenched by adding ice-cooled water (60 mL; very slowly), and the product was extracted with dichloromethane (20 mL). The combined organic phases were dried using sodium sulfate, and the solvent was evaporated under vacuum. Finally, the product was purified by column chromatography using a mixture of ethyl acetate/heptane to afford the corresponding hydroxylated compound.

Substitution of Bromine with Amine: The compound was prepared using literature procedure with some modification [50]. Compound 7u was dissolved in anhydrous DMSO (30 mL) and CuI (0.2 eq), L-Proline (0.5 eq), and Potassium carbonate (3 eq) were added to it under argon at room temperature. After stirring for 10 min, 28 % ammonium hydroxide (1 mL) was added, and the reaction mixture was heated to 85 °C for 20 h until the bromide was consumed as indicated by TLC. After cooling the reaction mixture to room temperature, it was quenched by adding water (50 mL) and extracted with ethyl acetate (50 mL x 3). The combined organic layers were washed with brine, dried over sodium sulfate, and evaporated under reduced pressure. The resulting residue was purified by silica gel chromatography to afford the corresponding primary aryl

amine

Substitution of Bromine with Aryls [51]: Compound 7u was dissolved in a mixture of THF (20 mL) and H_2O (2 mL) and $Pd(OAc)_2$ (0.1 eq), Phenylboronic acid (1.5 eq) and Na_2CO_3 was added to it at room temperature. The reaction mixture was then stirred for 12 h at 65 °C until the complete consumption of bromide as indicated by TLC and LC-MS. After cooling the crude mixture to room temperature, it was filtered, and the filtrate was extracted with ethyl acetate (50 mL x 3). The organic layer was washed with brine, dried over sodium sulfate, and evaporated under reduced pressure. The resulting residue was purified by silica gel chromatography to afford the corresponding aryls (45 % yield). All final compounds (7a-7v) were determined to be >95 % pure by analytical HRMS. The purity traces are provided in the Supplementary information.

The analytical data of all the synthesized final compounds **7a-v** are described below. A consolidated summary of structures, yields, HRMS purity and biological activities of all analogs (**7a-7v**) is provided in Table **52**.

2-(2-chloro-6-fluorobenzyl)-N-(furan-2-ylmethyl)-1-oxo-1,2-dihydroisoquinoline-7-carboxamide (7a): This compound was prepared according to the general procedure for coupling. (white powder; 78 %). $^1\mathrm{H}$ NMR (400 MHz, DMSO- d_6) δ ppm 4.48 (d, J=5.62 Hz, 2H) 5.32 (s, 2H) 6.26–6.31 (m, 1H) 6.38–6.41 (m, 1H) 6.68 (d, J=7.46 Hz, 1H) 7.21–7.28 (m, 1H) 7.37 (d, J=7.58 Hz, 1H) 7.39–7.46 (m, 1H) 7.46–7.50 (m, 1H) 7.58 (d, J=0.86 Hz, 1H) 7.72 (d, J=8.31 Hz, 1H) 8.11–8.17 (m, 1H) 8.73 (s, 1H) 9.20–9.25 (m, 1H) $^{13}\mathrm{C}$ NMR (100 MHz, DMSO- d_6) δ ppm 165.32, 162.79, 160.81, 160.31, 152.32, 142.03, 138.92, 134.47, 132.06, 131.03, 126.50, 126.31, 125.78, 124.78, 122.03, 114.89, 114.67, 110.47, 106.92, 104.71, 44.21, 36.13; HRMS (ESI⁺) m/z [M+H]⁺ calc. for $\mathrm{C}_{22}\mathrm{H}_{17}\mathrm{ClFN}_2\mathrm{O}_3$: 411.0907 found: 411.0904.

N-(*furan-2-ylmethyl*)-1-oxo-2-(2-chloro-6-fluoro)benzyl-1,2,3,4-tetra-hydroisoquinoline-7-carboxamide (*7b*): This compound was prepared according to the general procedure for coupling. (white powder; 80 %).

¹H NMR (400 MHz, DMSO- d_6) δ ppm 2.95 (t, J = 6.48 Hz, 2H) 3.43 (t, J = 6.54 Hz, 2H) 4.47 (d, J = 5.50 Hz, 2H) 4.90 (s, 2H) 6.28 (d, J = 2.81 Hz, 1H) 6.40 (dd, J = 3.06, 1.83 Hz, 1H) 7.24–7.30 (m, 1H) 7.35–7.47 (m, 3H) 7.59 (d, J = 0.86 Hz, 1H) 7.96 (dd, J = 7.89, 1.77 Hz, 1H) 8.43 (d, J = 1.59 Hz, 1H) 9.14 (s, 1H); ¹³C NMR (100 MHz, cdcl₃) δ ppm 165.15; 162.40, 160.21, 152.16, 141.79, 141.47, 134.69, 132.59, 130.32, 128.66, 127.31, 126.31, 125.57, 122.09, 114.61, 114.38, 110.25, 106.64, 44.23, 41.11, 35.86, 27.04; HRMS (ESI⁺) m/z [M+H]⁺ calc. for C₂₂H₁₉FN₂O₃Cl: 413.1063 found: 413.1065.

1-(2-chloro-6-fluorobenzyl)-N-(furan-2-ylmethyl)-2-oxo-1,2,3,4-tetra-hydroquinoline-6-carboxamide (7c): This compound was prepared according to the general procedure for coupling. (white powder; 86 %). 1 H NMR (400 MHz, CDCl₃) δ 7.61 (d, J=1.56 Hz, 1H), 7.52 (dd, J=1.96, 8.61 Hz, 1H), 7.34–7.37 (m, 1H), 7.11–7.18 (m, 2H), 6.98 (d, J=8.22 Hz, 1H), 6.86–6.93 (m, 1H), 6.37 (t, J=5.09 Hz, 1H), 6.31–6.34 (m, 1H), 6.27 (d, J=3.52 Hz, 1H), 5.43 (s, 2H), 4.59 (d, J=5.48 Hz, 2H), 2.91–2.97 (m, 2H), 2.68–2.76 (m, 2H); 13 C NMR (100 MHz, CDCl₃) δ 170.66, 166.67, 163.22, 160.73, 151.39, 142.60, 141.91, 135.17, 129.77, 128.81, 127.97, 127.27, 126.32, 115.46, 115.00, 114.77, 110.80, 108.03, 38.10, 37.23, 32.20, 25.36. HRMS (ESI⁺) m/z [M+H]⁺ calc. for C₂₂H₁₉ClFN₂O₃: 413.1063 found: 413.1066.

1-(2-chloro-6-fluorobenzyl)-N-(furan-2-ylmethyl)-2-oxo-1,2,3,4-tetra-hydroquinoline-5-carboxamide (7d): This compound was prepared according to the general procedure for coupling. (white powder; 80 %). 1 H NMR (400 MHz, cdcl₃) δ 7.35–7.38 (m, 1H), 7.09–7.15 (m, 3H), 7.01–7.07 (m, 2H), 6.87–6.93 (m, 1H), 6.33–6.35 (m, 1H), 6.29 (d, J = 3.13 Hz, 1H), 6.21 (t, J = 5.28 Hz, 1H), 5.40 (s, 2H), 4.59 (d, J = 5.87 Hz, 2H), 3.05 (dd, J = 6.26, 8.22 Hz, 2H), 2.65 (dd, J = 6.26, 8.22 Hz, 2H; 13 C NMR (100 MHz, cdcl₃) δ 170.56, 168.58, 162.93, 160.44, 150.73, 142.35, 139.61, 135.30, 134.92, 129.25, 127.02, 126.45, 125.88, 121.37, 117.25, 114.65, 110.52, 107.75, 37.68, 36.87, 31.65, 21.85. HRMS (ESI $^+$) m/z [M+H] $^+$ calc. for $C_{22}H_{19}$ ClFN₂O₃: 413.1063 found:

413,1069.

4-(2-chloro-6-fluorobenzyl)-N-(furan-2-ylmethyl)-3-oxo-3,4-dihydro-2H-benzo[b] [1,4]thiazine-2-carboxamide (7e): This compound was prepared according to the general procedure for coupling. (white powder; 73 %). 1 H NMR (400 MHz, DMSO-d₆) δ 10.45–10.62 (m, 1H), 7.70 (br. s., 1H), 7.03–7.20 (m, 5H), 6.82–6.99 (m, 3H), 6.04–6.17 (m, 1H), 5.68 (d, J=8.07 Hz, 1H), 3.98–4.31 (m, 2H), 3.42–3.78 (m, 2H) 13 C NMR (100 MHz, DMSO-d₆) δ 166.29, 165.48, 162.78, 160.3, 149.96, 141.23, 135.97, 129.01, 127.07, 124.82, 122.78, 121.17, 117.33, 116.68, 113.43, 113.20, 109.65, 106.31, 54.96, 36.37, 31.08; HRMS (ESI⁺) m/z [M+H]⁺ calc. for $\rm C_{21}H_{17}{\rm ClFN}_2O_3{\rm S}{\rm :}$ 431.0627 found: 431.0629.

4-(2-bromo-6-fluoro)benzyl-N-(furan-2-ylmethyl)-3-oxo-3,4-dihydro-2H-1,4-benzothiazine-6-carboxamide (*Tf*): This compound was prepared according to the general procedure for coupling. (white powder; 75 %).
¹H NMR (400 MHz, DMSO-d₆) δ 8.94 (t, J = 5.56 Hz, 1H), 7.76 (s, 1H), 7.58 (s, 1H), 7.46–7.53 (m, 2H), 7.41 (d, J = 7.82 Hz, 1H), 7.18–7.25 (m, 1H), 7.09–7.17 (m, 1H), 6.37–6.44 (m, 1H), 6.26 (d, J = 3.06 Hz, 1H), 5.35 (s, 2H), 4.46 (d, J = 5.62 Hz, 2H), 3.57 (s, 2H).
¹³C NMR (100 MHz, DMSO-d₆) δ 165.47, 165.03, 162.28, 159.78, 152.24, 142.04, 138.75, 132.73, 130.43, 128.98, 128.04, 123.99, 123.52, 123.38, 122.0, 117.47, 115.30, 110.46, 106.88, 42.91, 36.05, 30.78; HRMS (ESI⁺) m/z [M+H]⁺ calc. for C₂₁H₁₇BrFN₂O₃S: 475.0122, found: 475.01227.

Methyl 3-fluoro-2-((6-((furan-2-ylmethyl)carbamoyl)-3-oxo-2,3-dihydro-4H-benzo[b] [1,4]thiazin-4-yl)methyl)benzoate (7g): This compound was prepared according to the general procedure for coupling. (white powder; 82 %). 1 H NMR (400 MHz, CDCl₃) δ 7.67 (s, 1H), 7.38 (dd, J=15.3, 7.9 Hz, 2H), 7.32 (d, J=0.9 Hz, 1H), 7.28 (d, J=8.0 Hz, 1H), 7.15 (td, J=8.0, 5.4 Hz, 1H), 7.05–6.95 (m, 1H), 6.64 (s, 1H), 6.32–6.26 (m, 1H), 6.20 (d, J=2.9 Hz, 1H), 5.63 (s, 2H), 4.52 (d, J=5.3 Hz, 2H), 3.81 (s, 3H), 3.36 (s, 2H); 13 C NMR (100 MHz, cdcl₃) δ 167.70, 167.67, 165.74, 160.34, 151.30, 142.09, 142.06, 138.42, 129.04, 128.77, 128.52, 128.48, 122.45, 117.11, 117.09, 110.49, 110.45, 107.57, 52.79, 39.40, 39.36, 36.90, 31.74; HRMS (ESI⁺) m/z [M+H]⁺ calc. for C₂₃H₂₀FN₂O₅S: 455.1072 found: 455.1076.

4-(2-fluoro-6-nitrobenzyl)-N-(furan-2-ylmethyl)-3-oxo-3,4-dihydro-2H-benzo[b] [1,4]thiazine-6-carboxamide (7h): This compound was prepared according to the general procedure for amidation coupling. (white powder; 77 %). 1 H NMR (400 MHz, DMSO- d_6) δ 9.01 (t, J=5.62 Hz, 1H), 7.91 (s, 1H), 7.69–7.78 (m, 1H), 7.46–7.63 (m, 5H), 6.36–6.45 (m, 1H), 6.29 (d, J=2.93 Hz, 1H), 5.47 (s, 2H), 4.49 (d, J=5.62 Hz, 2H), 3.46 (s, 2H); 13 C NMR (100 MHz, DMSO- d_6) δ 166.17, 164.96, 161.94, 159.44, 152.21, 150.32, 142.08, 139.42, 132.80, 130.05, 128.18, 127.77, 122.44, 120.39, 119.47, 119.29, 117.01, 110.47, 106.97, 36.05, 30.56; HRMS (ESI⁺) m/z [M+H]⁺ calc. for C₂₁H₁₇FN₃O₅S: 442.0868 found: 442.0866.

4-(2-amino-6-fluorobenzyl)-N-(furan-2-ylmethyl)-3-oxo-3,4-dihydro-2H-benzo[b] [1,4]thiazine-6-carboxamide (7i): This compound was prepared according to the general procedure for coupling. (yellow powder; 81 %). $^1{\rm H}$ NMR (400 MHz, DMSO-d₆) δ 8.88 (t, J=5.62 Hz, 1H), 7.94 (s, 1H), 7.59 (d, J=0.73 Hz, 1H), 7.40–7.52 (m, 2H), 6.79–6.95 (m, 1H), 6.35–6.45 (m, 2H), 6.27 (d, J=2.93 Hz, 1H), 6.17 (dd, J=8.62, 9.96 Hz, 1H), 5.45 (s, 2H), 5.22 (s, 2H), 4.48 (d, J=5.50 Hz, 2H), 3.59 (s, 2H); $^{13}{\rm C}$ NMR (100 MHz, DMSO-d₆) δ 166.22, 165.03, 163.16, 160.75, 152.28, 148.87, 142.03, 138.02, 132.54, 129.25, 128.33, 128.00, 122.10, 118.01, 110.89, 110.46, 106.76, 106.09, 102.42, 36.08, 30.70; HRMS (ESI⁺) m/z [M+H]⁺ calc. for C₂₁H₁₉FN₃O₃S: 412.1126 found: 412.1121.

4-(2-fluoro-6-methoxybenzyl)-N-(furan-2-ylmethyl)-2-methyl-3-oxo-3,4-dihydro-2H-benzo[b] [1,4]thiazine-6-carboxamide (7j): This compound was prepared according to the general procedure for coupling. (white powder; 87 %). 1 H NMR (400 MHz, cdcl₃) δ 7.56 (d, J=1.5 Hz, 1H), 7.40–7.38 (m, 1H), 7.33 (dd, J=8.0, 1.5 Hz, 1H), 7.27 (d, J=7.9 Hz, 1H), 7.07 (td, J=8.3, 6.8 Hz, 1H), 6.56–6.45 (m, 3H), 6.35 (dd, J=3.1, 2.0 Hz, 1H), 6.28 (d, J=3.2 Hz, 1H), 5.39 (dd, J=56.8, 15.4 Hz, 2H), 4.59 (d, J=5.4 Hz, 2H), 3.73 (s, 3H), 3.52 (q, J=7.0 Hz, 1H), 1.46 (d, J=7.1 Hz, 3H); 13 C NMR (101 MHz, cdcl₃) δ 167.40, 166.21, 163.03,

160.64, 158.75, 151.07 (s), 142.29 (m), 137.84, 132.42, 128.69 (m),121.94 (d), 116.92 (m), 111.78 (d), 110.75 (d), 110.40 (d), 108.38 (s), 107.98 (m), 106.84 (m), 56.28(d), 38.39, 38.05, 37.03, 15.31(d); HRMS (ESI⁺) m/z [M+H]⁺ calc. for $C_{23}H_{22}FN_2O_4S$: 441.1279 found: 441.1276.

4-(2-fluoro-6-hydroxybenzyl)-3-oxo-N-(2,4,6-trifluorobenzyl)-3,4-dihydro-2H-benzo[b] [1,4]thiazine-7-carboxamide (7k): This compound was prepared according to the general procedure for deprotection of methyl ether with BBr₃. (yellowish powder; 67 %). 1 H NMR (400 MHz, cd₃od) δ 7.83 (s, 1H), 7.33 (d, J = 2.1 Hz, 2H), 6.95 (dd, J = 14.9, 8.2 Hz, 1H), 6.86 (t, J = 8.4 Hz, 2H), 6.50 (d, J = 8.2 Hz, 1H), 6.38 (t, J = 9.2 Hz, 1H), 5.35 (s, 2H), 4.58 (s, 2H), 3.46 (s, 2H). 13 C NMR (101 MHz, cd₃od) δ 167.41, 166.15, 163.38, 160.94, 157.03, 138.24, 132.34, 129.29, 128.90, 127.63, 121.84 (d, 2C), 118.07 (d, 2C), 110.81, 109.84 (d, 2C), 105.73, 99.75, 99.49, 36.32, 31.14, 30.84; HRMS (ESI⁺) m/z [M+H]⁺ calc. for C₂₃H₁₇F₄N₂O₃S: 477.0891 found: 477.0898.

4-(2-fluoro-6-methoxybenzyl)-3-oxo-N-(2,4,6-trifluorobenzyl)-3,4-dihydro-2H-benzo[b] [1,4]thiazine-7-carboxamide (7l): This compound was prepared according to the general procedure for amidation via HATU coupling. (white powder; 87 %). 1 H NMR (400 MHz, cdcl₃) δ7.54 (d, J=1.7 Hz, 1H), 7.33–7.22 (m, 2H), 7.06 (dd, J=8.4, 1.7 Hz, 1H), 6.68 (dd, J=8.6, 7.6 Hz, 2H), 6.57 (s, 1H NH peak), 6.55–6.43 (m, 2H), 5.35 (s, 2H), 4.62 (d, J=5.6 Hz, 2H), 3.74 (s, 3H), 3.41 (s, 2H); 13 C NMR (101 MHz, cdcl₃) δ 166.02, 164.86, 162.99 (t), 161.07, 160.51 (t), 158.89 (d), 138.24, 132.39, 129.50, 128.79, 122.00 (d), 117.16, 117.05 (d), 111.46 (d), 110.19, 108.07, 107.85, 106.76, 100.61, 100.18 (d), 56.24 (d), 36.27, 36.24, 31.62. HRMS (ESI⁺) m/z [M+H]⁺ calc. for C₂₄H₁₉F₄N₂O₃S: 491.1048 found: 491.1050.

4-(2-amino-6-fluorobenzyl)-3-oxo-N-(2,4,6-trifluorobenzyl)-3,4-dihydro-2H-benzo[b] [1,4]thiazine-6-carboxamide (7 m): This compound was prepared according to the general procedure for coupling. (white powder; 67 %). ¹H NMR (400 MHz, DMSO- d_6) δ 8.79 (t, J=5.07 Hz, 1H), 7.91 (s, 1H), 7.37–7.51 (m, 2H), 7.10–7.25 (m, 2H), 6.80–6.96 (m, 1H), 6.40 (d, J=8.19 Hz, 1H), 6.16 (dd, J=8.62, 10.09 Hz, 1H), 5.43 (br. s., 2H), 5.21 (s, 2H), 4.48 (d, J=5.01 Hz, 2H), 3.58 (s, 2H); ¹³C NMR (100 MHz, DMSO- d_6) δ 166.29, 164.98, 163.16, 162.54, 160.75, 159.92, 148.81, 137.97, 132.43, 129.27, 128.36, 127.96, 122.13, 118.06, 110.08, 105.98, 105.83, 102.33, 102.10, 100.43, 100.14, 37.03, 31.16, 30.71; HRMS (ESI⁺) m/z [M+H]⁺ calc. for C₂₃H₁₈F₄N₃O₂S: 476.1051 found: 476.1052.

4-(2-fluoro-6-nitrobenzyl)-3-oxo-N-(2,4,6-trifluorobenzyl)-3,4-dihydro-2H-benzo[b] [1,4]thiazine-6-carboxamide (7n): This compound was prepared according to the general procedure for coupling. (white powder; 85 %). 1 H NMR (400 MHz, DMSO- d_6) δ 8.90 (t, J=5.01 Hz, 1H), 7.85 (s, 1H), 7.68–7.75 (m, 1H), 7.46–7.59 (m, 4H), 7.19 (t, J=8.62 Hz, 2H), 5.45 (s, 2H), 4.48 (d, J=4.89 Hz, 2H), 3.45 (s, 2H); 13 C NMR (100 MHz, DMSO- d_6) δ 166.19, 164.91, 162.53, 161.93, 160.26, 159.44, 150.21, 139.34, 132.64, 129.98, 128.14, 127.83, 122.40, 120.23, 119.21, 117.02, 110.92, 100.76, 100.47, 100.19, 31.18, 30.58; HRMS (ESI⁺) m/z [M+H]⁺ calc. for $C_{23}H_{16}F_4N_3O_4S$: 506.0793 found: 506.0798.

4-(2-fluoro-6-hydroxybenzyl)-2-methyl-3-oxo-N-(2,4,6-tri-fluorobenzyl)-3,4-dihydro-2H-benzo[b] [1,4]thiazine-7-carboxamide (7ο): This compound was prepared according to the general procedure for deprotection of methyl ether with BBr₃ (yellowish powder; 73 %). 1 H NMR (400 MHz, cd3od) δ 7.83 (s, 1H), 7.43–7.27 (m, 2H), 6.97 (dd, J=15.2, 7.7 Hz, 1H), 6.80 (t, J=8.4 Hz, 2H), 6.53 (d, J=8.2 Hz, 1H), 6.44–6.29 (m, 1H), 5.36 (dd, J=35.9, 15.5 Hz, 2H), 4.59 (s, 2H), 3.56 (q, J=7.2 Hz, 1H), 1.42 (d, J=7.1 Hz, 3H); 13 C NMR (101 MHz, cd₃od) δ 168.44, 167.48, 163.31, 162.98, 161.12, 160.78, 157.09 (d), 137.88, 132.44, 128.84, 128.85, 121.74, 117.85, 117.74, 110.68, 110.17, 109.85, 105.80, 99.74, 86.70(d), 37.89 (d), 37.11, 31.14, 14.05 (d); HRMS (ESI⁺) m/z [M+H]⁺ calc. for C₂₄H₁₉F₄N₂O₃S: 491.1048 found 491.1045.

4-(2-fluoro-6-methoxybenzyl)-2-methyl-3-oxo-N-(2,4,6-tri-fluorobenzyl)-3,4-dihydro-2H-benzo[b] [1,4]thiazine-6-carboxamide (7p):

This compound was prepared according to the general procedure for coupling. (white powder; 77 %). $^1{\rm H}$ NMR (400 MHz, cdcl₃) δ 7.53 (d, J=1.4 Hz, 1H), 7.30 (dd, J=8.0, 1.4 Hz, 1H), 7.25 (dd, J=7.8, 4.3 Hz, 1H), 7.10–7.01 (m, 1H), 6.68 (t, J=8.1 Hz, 2H), 6.56 (t, J=5.3 Hz, 1H–NH), 6.50 (dd, J=18.1, 8.7 Hz, 2H), 5.35 (dd, J=58.3, 15.4 Hz, 2H), 4.62 (d, J=5.6 Hz, 2H), 3.73 (s, 3H), 3.50 (q, J=7.1 Hz, 1H), 1.44 (d, J=7.1 Hz, 3H); $^{13}{\rm C}$ NMR (101 MHz, cdcl₃) δ 167.38, 166.11, 163.00, 160.57 (d), 158.93, 137.34 (d), 132.34(d), 129.75(d), 129.06(m), 128.28, 127.63(d), 122.26, 121.61, 116.96, 116.54, 111.72(d), 110.21 (t), 107.90(dd), 106.80(m), 100.42 (m), 56.22(d), 38.38, 38.05, 31.65, 15.27(d); HRMS (ESI $^+$) m/z [M+H] $^+$ calc. for ${\rm C}_{25}{\rm H}_{21}{\rm F}_4{\rm N}_2{\rm O}_3{\rm S}$: 505.1204 found: 505.1201.

4-(2-fluoro-6-nitrobenzyl)-2-methyl-3-oxo-N-(2,4,6-trifluorobenzyl)-3,4-dihydro-2H-benzo[b] [1,4]thiazine-6-carboxamide (7q): This compound was prepared according to the general procedure for coupling. (white powder; 77 %). ¹H NMR (400 MHz, DMSO- d_6) δ 8.92 (s, 1H), 7.87 (s, 1H), 7.68–7.76 (m, 1H), 7.46–7.58 (m, 4H), 7.20 (t, J = 8.62 Hz, 2H), 5.31-5.54 (m, 2H), 4.48 (d, J = 4.89 Hz, 2H), 3.62 (d, J = 7.09 Hz, 1H), 1.21 (d, J = 7.09 Hz, 3H); ¹³C NMR (100 MHz, DMSO- d_6) δ 168.08, 164.95, 162.53, 161.92, 160.02, 159.43, 150.39, 138.86, 132.78, 130.06, 128.44, 126.56, 122.56, 120.43, 120.29, 119.49, 116.94, 110.93, 100.50, 37.21, 31.19, 14.51; HRMS (ESI⁺) m/z [M+H]⁺ calc. for C₂₄H₁₈F₄N₃O₄S: 520.0949 found: 520.0950.4-(2-amino-6-fluorobenzyl)-2-methyl-3-oxo-N-(2,4,6-trifluorobenzyl)-3,4-dihydro-2H-benzo [b] [1,4]thiazine-6-carboxamide (7r): This compound was prepared according to the general procedure for coupling. (yellow powder; 80 %). ¹H NMR (400 MHz, CHLOROFORM-d) δ 7.66 (s, 1H), 7.47–7.54 (m, 1H), 7.36 (d, J = 8.07 Hz, 1H), 6.91-7.01 (m, 1H), 6.69-6.78 (m, 2H), 6.59(br. s., 1H), 6.46 (d, J = 8.07 Hz, 1H), 6.20–6.32 (m, 1H), 5.35–5.44 (m, 1H), 5.22–5.33 (m, 1H), 4.67–4.74 (m, 2H), 3.52 (q, J = 7.05 Hz, 1H), 1.47 (d, J = 6.97 Hz, 3H); ¹³C NMR (100 MHz, DMSO- d_6) δ 169.06, 166.10, 163.39, 162.91, 161.00, 160.42, 137.18, 132.82, 130.12, 129.21, 128.11, 123.42, 116.41, 112.25, 110.11, 106.95, 104.34, 100.42, 38.17, 37.47, 31.69, 29.01, 22.68, 14.78; HRMS (ESI⁺) m/z $[M+H]^+$ calc. for $C_{24}H_{20}F_4N_3O_2S$: 490.1207 found: 490.1209.

7-bromo-4-(2-fluoro-6-methoxybenzyl)-3-oxo-N-(2,4,6-tri-fluorobenzyl)-3,4-dihydro-2H-benzo[b] [1,4]thiazine-6-carboxamide (7s): This compound was prepared according to the general procedure for coupling. (yellow powder; 78 %). ¹H NMR (400 MHz, DMSO- d_6) δ 8.82 (t, J=5.2 Hz, 1H), 7.62 (s, 1H), 7.31–7.15 (m, 4H), 6.78 (d, J=8.4 Hz, 1H), 6.67 (dd, J=9.9, 8.4 Hz, 1H), 5.22 (s, 2H), 4.40 (d, J=5.2 Hz, 2H), 3.70 (s, 3H), 3.56 (s, 2H); ¹³C NMR (101 MHz, DMSO- d_6) δ 166.50, 165.06, 162.94, 160.49, 158.96, 158.88, 138.03, 137.02, 131.82, 130.34, 130.23, 127.56, 119.02, 112.67, 111.53, 111.37, 108.33, 108.11, 107.64, 100.90 (t), 56.32, 36.05, 31.24, 30.97; HRMS (ESI⁺) m/z [M+H]⁺ calc. for C₂₄H₁₈BrF₄N₃O₄S: 569.0153 found: 569.0154.

Methyl 8-amino-4-(2-fluoro-6-methoxybenzyl)-3-oxo-3,4-dihydro-2H-benzo[b] [1,4]thiazine-6 carboxylate (7t): This compound was prepared according to the general procedure for the substitution of bromine with amine. 49 (white powder; 47 %). 1 H NMR (400 MHz, DMSO- d_6) δ 8.55 (s, 1H), 7.17 (t, J=8.8 Hz, 3H), 7.07–6.96 (m, 1H), 6.79–6.74 (m, 1H), 6.71 (d, J=8.4 Hz, 1H), 6.60 (t, J=9.1 Hz, 1H), 5.21 (d, J=6.2 Hz, 4H), 4.39 (d, J=5.0 Hz, 2H), 3.66 (s, 3H), 3.42 (s, 2H); 13 C NMR (101 MHz, DMSO) δ 166.72, 165.54, 160.47, 159.16, 159.08, 145.98, 139.29, 133.28, 129.89, 129.79, 112.35, 112.19, 111.38, 109.01, 108.15, 107.93, 107.41, 106.62, 101.16, 100.89 (t), 56.41, 36.38, 31.49, 31.24; HRMS (ESI⁺) m/z [M+H]⁺ calc. for C₂₄H₂₀F₄N₃O₃S: 506.1157 found: 506.1152.

7-bromo-4-(2-fluoro-6-hydroxybenzyl)-3-oxo-N-(2,4,6-tri-fluorobenzyl)-3,4-dihydro-2H-benzo[b] [1,4]thiazine-6-carboxamide (7u): This compound was synthesized following the general procedure for coupling and obtained as a yellow solid (75 %). $^{1}\mathrm{H}$ NMR (400 MHz, DMSO-d₆) δ 10.20 (s, 1H), 8.76 (s, 1H), 7.63 (d, J=1.2 Hz, 1H), 7.26 (s, 1H), 7.18 (t, J=8.5 Hz, 2H), 7.05 (q, J=7.8 Hz, 1H), 6.61 (d, J=8.2 Hz, 1H), 6.48 (t, J=9.3 Hz, 1H), 5.19 (s, 2H), 4.40 (d, J=5.2 Hz, 2H), 3.56 (s, 2H); $^{13}\mathrm{C}$ NMR (101 MHz, DMSO-d₆) δ 166.35, 165.10, 163.29,

160.86, 157.65, 157.57, 138.24, 136.97, 131.83, 129.68, 129.57, 127.30, 112.64, 111.66, 111.63, 110.03, 109.88, 106.35, 110.93, 100.86 (m), 36.88, 31.26, 30.88; HRMS (ESI $^+$) m/z [M+H] $^+$ calc. for $C_{24}H_{16}BrF_4N_2O_3S$: 554.9996 found: 554.9999.

4-(2-fluoro-6-hydroxybenzyl)-3-oxo-7-phenyl-N-(2,4,6-tri-fluorobenzyl)-3,4-dihydro-2H-benzo[b] [1,4]thiazine-6-carboxamide (7ν): This compound was synthesized following the general procedure for the substitution of bromine with aryls 50 and obtained as a yellow solid (45 %). 1 H NMR (400 MHz, DMSO- d_{6}) δ 10.25 (s, 1H), 8.52 (t, J=5.5 Hz, 1H), 8.25 (t, J=5.4 Hz, 2H), 7.96 (s, 1H), 7.40–7.31 (m, 2H), 7.20 (s, 5H), 6.65 (d, J=8.2 Hz, 1H), 6.51 (t, J=9.4 Hz, 1H), 5.25 (s, 2H), 4.25 (s, 2H), 3.58 (s, 2H); 13 C NMR (101 MHz, DMSO- d_{6}) δ 169.36, 168.19, 165.30, 162.77, 160.35, 157.66, 157.59, 139.05, 137.86, 135.37, 134.31, 129.67, 129.56, 129.45, 128.41, 127.52, 125.11, 117.98, 111.66, 111.61, 111.57, 110.34, 110.19, 106.46, 106.24, 100.93 (t), 36.24, 30.61, 22.76; HRMS (ESI⁺) m/z [M+H]⁺ calc. for C₂₉H₂₁F₄N₂O₃S: 553.1204 found: 553.1208.

4.2. Biological evaluation

Cell Lines: Human fibroblast cell lines (THF-ISRE IRF3, THF-ISRE STING KO, and THF-ISRE TRIF/MAVS KO) were gifted to us by Dr. Victor DeFilippis from OHSU. Each of the cell lines were maintained in DMEM (Cytiva) media supplemented with 10 % heat-inactivated Fetal Bovine Serum (FBS- Cytiva) and 1X Penicillin/Streptomycin (Cytiva). Cells were kept at 37 $^{\circ}$ C with 5 $^{\circ}$ CO₂.

Luciferase Activity Screening: THF-ISRE IRF3 cell lines are human fibroblasts stably transfected with a luciferase reporter gene downstream of IRF3 transcription. Cells produce measurable luciferase upon activation of IRF3. Cells were cultured at a density of 15,000 for 28 h before treatment. Candidate compounds were formulated in DMSO to final concentration of 2 mg/mL and added to corresponding wells at 50 $\mu\text{M},$ 25 $\mu\text{M},$ 12.5 $\mu\text{M},$ and 6.25 μM concentrations. Each concentration was plated in triplicate. The treated cells were incubated for 24 h, after which Promega Steady-Glo reagent was added at a 1:1 vol ratio and luciferase was measured using Molecular Devices iD5 plate reader.

The average relative luminescence units (RLU) from each compound were calculated and normalized to the 1 % DMSO control. Results are displayed as fold-change over DMSO. Compounds were considered active if they induce \geq 2-fold luciferase activity compared to DMSO. **G10** was used as a positive control.

Secondary screening was performed to evaluate specificity for human STING using THF-ISRE STING KO cells (STING $^{-/-}$ lacks STING pathway) and THF-ISRE TRIF KO/MAVS KO cells (TRIF/MAVS $^{-/-}$ has only STING pathway). IFN- β was used as a positive control for THF-ISRE STING $^{-/-}$ cells. Cells were expanded, treated, and luciferase activity measured as in the primary screen.

In vivo experimental: Animal studies were carried out in an OLAW and AAALAC accredited vivarium in accordance with University of Montana's IACUC guidelines for the care and use of laboratory animals. 7k is a human-selective STING agonist. Therefore, to characterize the immune response to 7k, we utilized C57BL/6 humanized STING (huS-TING) mice, in which the murine STING coding region has been replaced with that of the wildtype human allele. Both Male and Female mice, between the ages of 6-12 weeks, were randomized into groups of 8. The HuSTING mice were either unimmunized or intramuscularly immunized and boosted (at a two week interval) with 50 µL of either detergent-split A/Victoria/210/2009 (H3N2, A/Vic) alone or in combination with 7k formulated in DMSO. Previous in vivo studies had determined 1 % DMSO alone group had immune responses similar to naïve mice and the optimum dose for 7k was 20 μg with 1 % DMSO (data not shown). Two weeks post-boost, blood and spleens were collected to evaluate A/Vicspecific IgG titers and Th cell responses, respectively. A/Vic-specific serum antibody titers were measured by ELISA. Capture plates were prepared by coating with 0.3 µg of A/Vic and incubating overnight at 4 °C. Serum samples were initially diluted in the top row of the capture

plate and then serially diluted 1:3 down the plate. After 2 h of incubation at 37 °C, plates were treated with HRP-conjugated secondary antibody for 1 h. Then TMB substrate was added. The substrate color reaction was stopped after 20 min. The OD450 was measured on a SpectraMax iD5 plate reader from Molecular Devices. Data was analyzed using XL-Fit and Prism. To measure splenic Th cell cytokine responses, splenocytes were plated at 5 \times 106 cells/well, restimulated with 1 μg of A/Vic antigen for 72 h at 37 °C with 5 % CO2. Supernatants were then collected to be analyzed using a custom cytokine panel from Meso Scale Diagnostics, which included Th1 cytokines (IFNy, TNFa, and IL-2), Th2 cytokines (IL-4 and IL-5), and the Th17 cytokine, IL-17A. The plate was read using Meso QuickPlex reader and analyzed the date using Prism (version 10).

4.3. Molecular docking

The 3D structure of the target proteins, STING CBD complexed with diABZI (PDB ID: 8STH) and STING TMD complexed with C53 (PDB ID: 7SII) were obtained from the Protein Data Bank [52]. Proteins preparations were performed in AutoDock Tools [53]. For the protein, water molecules were removed, hydrogens were added, and Gasteiger charges were assigned prior to saving the file in PDBQT format. Docking grids were centered on the co-crystallized ligand positions with a spacing of 10 Å. The 3D structures of all compounds were drawn in Discovery Studio Visualizer [54] and then subject to energy minimization. The ligand structures were then converted to PDBQT format using AutoDock Tools. Molecular docking analysis were performed using AutoDock Vina. The docking parameters 'exhaustiveness' was set to 9 and other parameters were set to 'default'. The docking results were visualized using Discovery Studio Visualizer.

CRediT authorship contribution statement

Ahmad Junaid: Writing – review & editing, Writing – original draft, Visualization, Software, Methodology, Investigation, Conceptualization. Uddav Pandey: Writing – review & editing, Visualization, Methodology, Investigation. Janine Ward: Writing – review & editing, Methodology, Investigation. Nilesh Meghani: Writing – review & editing. Shannon Miller: Writing – review & editing, Project administration, Methodology, Investigation. Austin Negron: Writing – review & editing. Kendal Ryter: Writing – review & editing. David Burkhart: Writing – review & editing, Funding acquisition, Conceptualization. Nobuyu Mizuno: Investigation, Methodology, Writing – review & editing. Victor R. DeFilippis: Writing – review & editing, Visualization, Supervision, Resources, Project administration, Methodology, Investigation, Funding acquisition, Conceptualization. Omer Rasheed: Writing – original draft, Visualization, Supervision, Software, Resources, Project administration, Methodology, Investigation, Conceptualization.

Funding

This work was funded by National Institutes of Health Grants HHSN272201400055C.

Declaration of competing interest

The authors declare that they have no known competing financial interests or personal relationships that could have appeared to influence the work reported in this paper.

Appendix A. Supplementary data

Supplementary data to this article can be found online at https://doi.org/10.1016/j.ejmech.2025.118201.

Data availability

SUPPORTING DATA IS PROVIDED AS ATTACHMENT

References

- Mikayla R. Thompson, John J. Kaminski, Evelyn A. Kurt-Jones, Katherine A. Fitzgerald, Pattern recognition receptors and the innate immune response to viral infection, Viruses 3 (6) (2011) 920, https://doi.org/10.3390/v3060920.
- [2] Danyang Li, Minghua Wu, Pattern recognition receptors in health and diseases, Signal Transduct. Targeted Ther. 6 (1) (2021) 291, https://doi.org/10.1038/ s41392-021-00687-0.
- [3] Lin Zhao, Jinlan Niu, Disong Feng, Xialu Wang, Rong Zhang, Immune functions of pattern recognition receptors in Lepidoptera, Front. Immunol. 14 (2023) 1203061, https://doi.org/10.3389/fimmu.2023.1203061.
- [4] Jeonghyun Ahn, Glen N. Barber, Self-DNA, STING-dependent signaling and the origins of autoinflammatory disease, Curr. Opin. Immunol. 31 (2014) 121–126, https://doi.org/10.1016/j.coi.2014.10.009.
- [5] Pu Gao, Manuel Ascano, Yang Wu, Winfried Barchet, Barbara L. Gaffney, Thomas Zillinger, Artem A. Serganov, et al., Cyclic [G (2', 5') pA (3', 5') p] is the metazoan second messenger produced by DNA-activated cyclic GMP-AMP synthase, Cell 153 (5) (2013) 1094–1107, https://doi.org/10.1016/j. cell.2013.04.046.
- [6] Elie J. Diner, Dara L. Burdette, Stephen C. Wilson, Kathryn M. Monroe, Colleen A. Kellenberger, Mamoru Hyodo, Yoshihiro Hayakawa, Ming C. Hammond, Russell E. Vance, "The innate immune DNA sensor cGAS produces a noncanonical cyclic dinucleotide that activates human STING.", Cell reports 3, no 5 (2013) 1355–1361, https://doi.org/10.1016/j.celrep.2013.05.009 [CrossRef Partial][doi and sti merged, Check "vol" partially styled, Check au5,stl,vol,doi,au7 style(s) incorrectly styled in the reference, Check multiple stl, vol, iss, adate, first-page, last-page].
- [7] Zhe Ma, Blossom Damania, The cGAS-STING defense pathway and its counteraction by viruses, Cell Host Microbe 19 (2) (2016) 150–158, https://doi. org/10.1016/j.chom.2016.01.010.
- [8] Fabio V. Marinho, Sulayman Benmerzoug, Sergio C. Oliveira, Bernhard Ryffel, Valerie FJ. Quesniaux, The emerging roles of STING in bacterial infections, Trends Microbiol. 25 (11) (2017) 906–918. https://doi.org/10.1016/j.tim.2017.05.008.
- [9] John Kwon, Samuel F. Bakhoum, The cytosolic DNA-sensing cGAS-STING pathway in cancer, Cancer Discov. 10 (1) (2020) 26–39, https://doi.org/10.1158/2159-8290.CD-19-0761.
- [10] Tomohiko Tamura, Hideyuki Yanai, David Savitsky, Tadatsugu Taniguchi, The IRF family transcription factors in immunity and oncogenesis, Annu. Rev. Immunol. 26 (1) (2008) 535–584, https://doi.org/10.1146/annurev. immunol.26.021607.090400.
- [11] Qian Zhang, Michael J. Lenardo, David Baltimore, 30 years of NF-κB: a blossoming of relevance to human pathobiology, Cell 168 (1) (2017) 37–57, https://doi.org/ 10.1016/j.cell.2016.12.012.
- [12] Marlene F. Laursen, Esben Christensen, Laura LT. Degn, Kasper Jønsson, Martin R. Jakobsen, Ralf Agger, Emil Kofod-Olsen, CD11c-targeted delivery of DNA to dendritic cells leads to cGAS-and STING-dependent maturation, J. Immunother. 41 (1) (2018) 9–18, https://doi.org/10.1097/CJI.00000000000000195.
- [13] Fabio V. Marinho, Sulayman Benmerzoug, Stephanie Rose, Priscila C. Campos, João T. Marques, André Báfica, Glen Barber, Bernhard Ryffel, Sergio C. Oliveira, Valerie FJ. Quesniaux, The cGAS/STING pathway is important for dendritic cell activation but is not essential to induce protective immunity against mycobacterium tuberculosis infection, J. Innate Immun. 10 (3) (2018) 239–252, https://doi.org/10.1159/000488952.
- [14] Ralph E. Vatner, M. Janssen Edith, STING, DCs and the link between innate and adaptive tumor immunity, Mol. Immunol. 110 (2019) 13–23, https://doi.org/ 10.1016/j.molimm.2017.12.001.
- [15] Jocelyn T. Kim, Yarong Liu, Rajan P. Kulkarni, Kevin K. Lee, Bingbing Dai, Geoffrey Lovely, Yong Ouyang, Pin Wang, Lili Yang, David Baltimore, Dendritic cell-targeted lentiviral vector immunization uses pseudotransduction and DNAmediated STING and cGAS activation, Science immunology 2 (13) (2017) eaal1329, https://doi.org/10.1126/sciimmunol.aal1329.
- [16] Jr Dubensky, W. Thomas, David B. Kanne, Meredith L. Leong, Rationale, progress and development of vaccines utilizing STING-activating cyclic dinucleotide adjuvants, Therapeutic advances in vaccines 1 (4) (2013) 131–143, https://doi. org/10.1177/2051013613501988.
- [17] Erik Van Dis, Kimberly M. Sogi, Chris S. Rae, Kelsey E. Sivick, Natalie H. Surh, Meredith L. Leong, David B. Kanne, et al., STING-activating adjuvants elicit a Th17 immune response and protect against Mycobacterium tuberculosis infection, Cell Rep. 23 (5) (2018) 1435–1447, https://doi.org/10.1016/j.celrep.2018.04.003.
- [18] Aysa Rezabakhsh, M. Reza Sadaie, Alireza Ala, Yousef Roosta, Solomon Habtemariam, Adeleh Sahebnasagh, Mohammad Rafi Khezri, STING agonists as promising vaccine adjuvants to boost immunogenicity against SARSrelated coronavirus derived infection: possible role of autophagy, Cell Commun. Signal. 22 (1) (2024) 305, https://doi.org/10.1186/s12964-024-01680-0.
- [19] Van Herck, Simon, Bing Feng, Li Tang, Delivery of STING agonists for adjuvanting subunit vaccines, Adv. Drug Deliv. Rev. 179 (2021) 114020, https://doi.org/ 10.1016/j.addr.2021.114020.
- [20] Xinyu Tian, Jiayuan Ai, Xiaohe Tian, Wei Xiawei, cGAS-STING pathway agonists are promising vaccine adjuvants, Med. Res. Rev. 44 (4) (2024) 1768–1799, https://doi.org/10.1002/med.22016.

- [21] Yanru Shen, Weijin Huang, Jianhui Nie, Li Zhang, Progress Update on STING agonists as vaccine adjuvants, Vaccines 13 (4) (2025) 371, https://doi.org/ 10.3390/vaccines13040371.
- [22] Funda Meric-Bernstam, Randy F. Sweis, Stefan Kasper, Omid Hamid, Shailender Bhatia, Reinhard Dummer, Agostina Stradella, et al., Combination of the STING agonist MIW815 (ADU-S100) and PD-1 inhibitor spartalizumab in advanced/metastatic solid tumors or lymphomas: an open-label, multicenter, phase Ib study, Clin. Cancer Res. 29 (1) (2023) 110–121, https://doi.org/10.1158/ 1078-0432.CGR-22-2235.
- [23] Xiyuan Wang, Ancheng Shen, Yan Zhang, Xiaoxu Chen, Jian Ding, Ao Zhang, Meiyu Geng, Chunyong Ding, Zuoquan Xie, A novel STING agonist with systemic and durable anti-tumour activity, Clinical and Translational Discovery 3 (5) (2023) e231, https://doi.org/10.1002/ctd2.231.
- [24] Matthew Maddess, John McIntosh, Wonsuk Chang, Discovery and chemical development of uvelostinag (MK-1454): a therapeutic cyclic dinucleotide agonist of the stimulator of interferon gene, in: Complete Accounts of Integrated Drug Discovery and Development: Recent Examples from the Pharmaceutical Industry, 4, American Chemical Society, 2022, pp. 1–94, https://doi.org/10.1021/bk-2022-14/3 ch001
- [25] Qian Zeng, Min Liu, Ziqi Wang, Rongrong Zhou, Kelong Ai, Enhancing radiotherapy-induced anti-tumor immunity via nanoparticle-mediated STING agonist synergy, Mol. Cancer 24 (1) (2025) 176, https://doi.org/10.1186/s12943-025-02366-v.
- [26] Motedayen Aval, James E. Pease Leila, Rohini Sharma, David J. Pinato, Challenges and opportunities in the clinical development of STING agonists for cancer immunotherapy, J. Clin. Med. 9 (10) (2020) 3323, https://doi.org/10.3390/ jcm9103323.
- [27] Bo-Sheng Pan, Samanthi A. Perera, Jennifer A. Piesvaux, Jeremy P. Presland, Gottfried K. Schroeder, Jared N. Cumming, B. Wesley Trotter, et al., An orally available non-nucleotide STING agonist with antitumor activity, Science 369 (6506) (2020) eaba6098, https://doi.org/10.1126/science.aba6098.
- [28] Kyle M. Garland, Taylor L. Sheehy, John T. Wilson, Chemical and biomolecular strategies for STING pathway activation in cancer immunotherapy, Chem. Rev. 122 (6) (2022) 5977–6039, https://doi.org/10.1021/acs.chemrev.1c00750.
- [29] Sujeong Kim, Lingyin Li, Zoltan Maliga, Qian Yin, Hao Wu, Timothy J. Mitchison, Anticancer flavonoids are mouse-selective STING agonists, ACS Chem. Biol. 8 (7) (2013) 1396–1401, https://doi.org/10.1021/cb400264n.
- [30] Yang Wang, Jingwen Luo, Aqu Alu, Xuejiao Han, Yuquan Wei, Xiawei Wei, cGAS-STING pathway in cancer biotherapy, Mol. Cancer 19 (1) (2020) 136, https://doi.org/10.1186/s12943-020-01247-w.
- [31] Yanru Shen, Weijin Huang, Jianhui Nie, Li Zhang, Progress Update on STING agonists as vaccine adjuvants, Vaccines 13 (4) (2025) 371, https://doi.org/ 10.3390/vaccines13040371.
- [32] Daei Farshchi Adli, Amir, Rana Jahanban Esfahlan, Khaled Seidi, Sonia Samandari-Rad, Nosratollah Zarghami, An overview on Vadimezan (DMXAA): the vascular disrupting agent, Chem. Biol. Drug Des. 91 (5) (2018) 996–1006, https://doi.org/10.1111/cbdd.13166.
- [33] Joshi M. Ramanjulu, G. Scott Pesiridis, Jingsong Yang, Nestor Concha, Robert Singhaus, Shu-Yun Zhang, Jean-Luc Tran, et al., Design of amidobenzimidazole STING receptor agonists with systemic activity, Nature 564 (7736) (2018) 439–443, https://doi.org/10.1038/s41586-019-1265-5.
- [34] Emily N. Chin, Chenguang Yu, Vincent F. Vartabedian, Ying Jia, Manoj Kumar, Ana M. Gamo, William Vernier, et al., Antitumor activity of a systemic STING-activating non-nucleotide cGAMP mimetic, Science 369 (6506) (2020) 993–999, https://doi.org/10.1126/science.abb4255.
- [35] Fang Wang, Kai Fu, Yujue Wang, Can Pan, Xueping Wang, Zeyu Liu, Chuan Yang, et al., Small-molecule agents for cancer immunotherapy, Acta Pharm. Sin. B 14 (3) (2024) 905–952, https://doi.org/10.1016/j.apsb.2023.12.010.
- [36] Chang Shen, Peijia Xu, Changfa Zhang, Zhaoming Su, Bin Shan, Rui Li, Qibang Sui, et al., Structure–activity relationship study of 1 H-Pyrrole-3-carbonitrile derivatives as STING receptor agonists, ACS Med. Chem. Lett. 14 (8) (2023) 1079–1087. https://doi.org/10.1021/acsmedchemlett.3c00208.
- [37] Defen Lu, Guijun Shang, Jie Li, Yong Lu, Xiao-chen Bai, Xuewu Zhang, Activation of STING by targeting a pocket in the transmembrane domain, Nature 604 (7906) (2022) 557–562, https://doi.org/10.1038/s41586-022-04559-7.

- [38] Guijun Shang, Conggang Zhang, Zhijian J. Chen, Xiao-chen Bai, Xuewu Zhang, Cryo-EM structures of STING reveal its mechanism of activation by cyclic GMP-AMP, Nature 567 (7748) (2019) 389–393, https://doi.org/10.1038/s41586-019.098-5
- [39] Rongyao Zhou, Xiyuan Wang, Deqiang Zhang, Zhengsheng Zhan, · Wenhu Duan, Design, synthesis, and STING-agonistic activity of benzo [b] thiophene-2carboxamide derivatives, Mol. Divers. (2023) 1–10, https://doi.org/10.1007/ s11030-023-10736-1.
- [40] Behzad Hussain, Yufeng Xie, Uzma Jabeen, Defen Lu, Bo Yang, Changxin Wu, Guijun Shang, Activation of STING based on its structural features, Front. Immunol. 13 (2022) 808607, https://doi.org/10.3389/fimmu.2022.808607.
- [41] Yinfeng Xu, Qian Wang, Jun Wang, Chuying Qian, Yusha Wang, Sheng Lu, Lijiang Song, Zhengfu He, Wei Liu, Wei Wan, The cGAS-STING pathway activates transcription factor TFEB to stimulate lysosome biogenesis and pathogen clearance, Immunity 58 (2) (2025) 309–325, https://doi.org/10.1016/j. immuni.2024.11.017.
- [42] Tuozhi Huang, Chenglong Sun, Fenghe Du, Zhijian J. Chen, STING-induced noncanonical autophagy regulates endolysosomal homeostasis, Proc. Natl. Acad. Sci. 122 (8) (2025) e2415422122, https://doi.org/10.1073/pnas.2415422122.
- [43] Guijun Shang, Conggang Zhang, Zhijian J. Chen, Xiao-chen Bai, Xuewu Zhang, Cryo-EM structures of STING reveal its mechanism of activation by cyclic GMP-AMP, Nature 567 (7748) (2019) 389–393, https://doi.org/10.1038/s41586-019-098-5
- [44] Behzad Hussain, Yufeng Xie, Uzma Jabeen, Defen Lu, Bo Yang, Changxin Wu, Guijun Shang, Activation of STING based on its structural features, Front. Immunol. 13 (2022) 808607, https://doi.org/10.3389/fimmu.2022.808607.
- [45] Jinu Abraham, Sara Botto, Nobuyo Mizuno, Kara Pryke, Bryan Gall, Dylan Boehm, Tina M. Sali, et al., Characterization of a novel compound that stimulates STINGmediated innate immune activity in an allele-specific manner, Front. Immunol. 11 (2020) 1430, https://doi.org/10.3389/fimmu.2020.01430.
- [46] Monali Banerjee, Sandip Middya, Ritesh Shrivastava, Sourav Basu, Rajib Ghosh, David C. Pryde, Dharmendra B. Yadav, Arjun Surya, G10 is a direct activator of human STING, PLoS One 15 (9) (2020) e0237743, https://doi.org/10.1371/ journal.pone.0237743.
- [47] Jeremy R. Duvall, Joshua D. Thomas, Raghida A. Bukhalid, Kalli C. Catcott, Keith W. Bentley, Scott D. Collins, Timothy Eitas, et al., Discovery and optimization of a STING agonist platform for application in antibody drug conjugates, J. Med. Chem. 66 (15) (2023) 10715–10733, https://doi.org/10.1021/acs.jmedchem.3c00907;
 [b] Li Fu, Shaohua Shi, Jiacai Yi, Ningning Wang, Yuanhang He, Zhenxing Wu, Jinfu Peng, et al., ADMETlab 3.0: an updated comprehensive online ADMET prediction platform enhanced with broader coverage, improved performance, API functionality and decision support, Nucleic Acids Res. 52 (W1) (2024)
 W422—W431. https://doi.org/10.1093/nar/gkae236.
- [48] David C. Pryde, Sandip Middya, Monali Banerjee, Ritesh Shrivastava, Sourav Basu, Rajib Ghosh, Dharmendra B. Yadav, Surya Arjun, The discovery of potent small molecule activators of human STING, Eur. J. Med. Chem. 209 (2021) 112869, https://doi.org/10.1016/j.ejmech.2020.112869.
- [49] Nobuyo Mizuno, Jinu Abraham, Kevin Jimenez-Perez, Ian Rose, Laura Springgay, Dylan Boehm, Takeshi Ando, et al., Characterization of a novel transmembrane activating STING agonist using genetically humanized mice, bioRxiv (2025), https://doi.org/10.1101/2025.07.14.664814, 2025-07.PMID 40791406.
- [50] Liqin Jiang, Xu Lu, Hui Zhang, Yongwen Jiang, Dawei Ma, CuI/4-Hydro-l-proline as a more effective catalytic system for coupling of aryl bromides with N-boc hydrazine and aqueous ammonia, J. Org. Chem. 74 (12) (2009) 4542–4546, https://doi.org/10.1021/jo9006738.
- [51] Norio Miyaura, T. Yanagi, A.J.S.C. Suzuki, The palladium-catalyzed cross-coupling reaction of phenylboronic acid with haloarenes in the presence of bases, Synth. Commun. 11 (7) (1981) 513–519, https://doi.org/10.1080/00397918108063618.
- [52] Protein Data Bank. http://www.rcsb.org/pdb/home/home.do.
- [53] Garrett M. Morris, Ruth Huey, William Lindstrom, Michel F. Sanner, Richard K. Belew, David S. Goodsell, Arthur J. Olson, AutoDock4 and AutoDockTools4: automated docking with selective receptor flexibility, J. Comput. Chem. 30 (16) (2009) 2785–2791, https://doi.org/10.1002/jcc.21256.
- [54] Biovia, Dassault Systèmes, Discovery studio visualizer, San Diego, CA, USA 936, 2017, pp. 240–249. https://www.3ds.com/products/biovia/discovery-studio/visualization.